Satellite-Based Emission Inversion for Air Pollutants and Greenhouse Gases: A Review

Zhe JIANG, Jintai LIN, Tai-Long HE, Fei JIANG, Jianbing JIN, Kai QIN, Lu SHEN, Panpan YANG, Zengliang ZANG, Lin ZHANG, Yuzhong ZHANG, Bo ZHENG, Huiru ZHONG, Lei ZHU

Citation: Jiang, Z., J. T. Lin, T. L. He, et al., 2025: Satellite-based emission inversion for air pollutants and greenhouse gases: A review. *J. Meteor. Res.*, 39(5), 1–25, doi: https://doi.org/10.1007/s13351-025-4914-7

View online: http://jmr.cmsjournal.net/article/doi/10.1007/s13351-025-4914-7

Related articles that may interest you

Shortened Duration of Global Warming Slowdowns with Elevated Greenhouse Gas Emissions

Journal of Meteorological Research. 2021, 35(2), 225 https://doi.org/10.1007/s13351-021-0134-y

Forced Decadal Changes in Summer Precipitation Characteristics over China: The Roles of Greenhouse Gases and Anthropogenic Aerosols

Journal of Meteorological Research. 2020, 34(6), 1226 https://doi.org/10.1007/s13351-020-0060-4

Impacts of Atmospheric Boundary Layer Vertical Structure on Haze Pollution Observed by Tethered Balloon and Lidar

Journal of Meteorological Research. 2021, 35(1), 209 https://doi.org/10.1007/s13351-021-0076-4

Comparison of Two Air Pollution Episodes over Northeast China in Winter 2016/17 Using Ground-Based Lidar

Journal of Meteorological Research. 2018, 32(2), 313 https://doi.org/10.1007/s13351-018-7047-4

Relative Contributions of Boundary–Layer Meteorological Factors to the Explosive Growth of PM_{2.5} during the Red–Alert Heavy Pollution Episodes in Beijing in December 2016

Journal of Meteorological Research. 2017, 31(5), 809 https://doi.org/10.1007/s13351-017-7088-0

Influence of Intermittent Turbulence on Air Pollution and Its Dispersion in Winter 2016/2017 over Beijing, China

Journal of Meteorological Research. 2020, 34(1), 176 https://doi.org/10.1007/s13351-020-9128-4



Satellite-Based Emission Inversion for Air Pollutants and Greenhouse Gases: A Review

Zhe JIANG¹, Jintai LIN^{2*}, Tai-Long HE³, Fei JIANG⁴, Jianbing JIN⁵, Kai QIN⁶, Lu SHEN², Panpan YANG¹, Zengliang ZANG⁷, Lin ZHANG², Yuzhong ZHANG⁸, Bo ZHENG⁹, Huiru ZHONG², and Lei ZHU¹⁰

- 1 Institute of Surface-Earth System Science, School of Earth System Science, Tianjin University, Tianjin 300072, China 2 Laboratory for Climate and Ocean-Atmosphere Studies, Department of Atmospheric and Oceanic Sciences, School of Physics, Peking University, Beijing 100871, China
- 3 Department of Aeronautics and Astronautics, Massachusetts Institute of Technology, Cambridge, Massachusetts 02139, USA 4 International Institute for Earth System Science, Nanjing University, Nanjing 210023, China
- 5 School of Environmental Science and Engineering, Nanjing University of Information Science & Technology, Nanjing 211544, China 6 School of Environment and Spatial Informatics, China University of Mining and Technology, Xuzhou 221116, China 7 College of Meteorology and Oceanography, National University of Defense Technology, Changsha 410073, China
 - 8 School of Engineering, Westlake University, Hangzhou 310030, China 9 Tsinghua Shenzhen International Graduate School, Shenzhen 518055, China
 - 10 School of Environmental Science and Engineering, Southern University of Science and Technology, Shenzhen 518055, China

(Received 17 April 2025; in final form 18 September 2025)

ABSTRACT

Retrievals of satellite-observed emissions of atmospheric pollutants and greenhouse gases provide essential information and data for understanding the sources of these key atmospheric compositions and for implementing precise emission control measures. Over the past two decades, significant progress has been made in the field of emission inversion, with Chinese researchers playing a substantial role. In celebration of the 100th anniversary of the Chinese Meteorological Society and *Acta Meteorologica Sinica*, this paper systematically reviews the advances in satellite-based emission inversion research by Chinese scientists during this period. (1) Several widely used inversion methodologies, including data assimilation, local mass balance, Gaussian models, two-dimensional (2D) models, and machine learning, are briefly summarized. (2) Emission inversion studies focusing on major atmospheric pollutants—such as nitrogen oxides (NO_x), ammonia (NH₃), formaldehyde (HCHO), glyoxal (CHOCHO), sulfur dioxide (SO₂), and carbon monoxide (CO)—as well as greenhouse gases like carbon dioxide (CO₂) and methane (CH₄), are systematically elaborated. (3) Finally, the historical evolution of inversion methods and target species, challenges in current satellite-based emission inversion, and future research directions are discussed to promote more accurate quantification of atmospheric pollutants and greenhouse gas emissions. It is worth noting that contributions from Chinese researchers have provided critical scientific support to environmental protection and carbon neutrality efforts in China.

Key words: emission inversion, atmospheric pollutants, greenhouse gases, satellite observation

Citation: Jiang, Z., J. T. Lin, T. L. He, et al., 2025: Satellite-based emission inversion for air pollutants and green-house gases: A review. *J. Meteor. Res.*, 39(5), 1–25, https://doi.org/10.1007/s13351-025-4914-7.

1. Introduction

Anthropogenic activities, such as fossil fuel and biofuel combustion and fertilizer application, have resulted in a significant increase in the emission of air pollutants, including nitrogen oxides (NO_x), ammonia (NH_3), volatile organic compounds (VOCs), sulfur dioxide (SO_2), and carbon monoxide (CO). These pollutants harm the environment and can generate ozone (O_3) through photochemical reactions or form fine particulate matter (PM_{2.5}) via gas-to-particle conversion processes, posing serious threats to public health and ecosystems. Previous studies (Xu et al., 2023; Chen X. K. et al., 2024) estimated that over 1 million premature deaths may have occurred annually in China due to exposure to O₃ and PM_{2.5}, and the impacts are expected to exacerbate with the aging population. Moreover, anthropogenic activities have resulted in a rapid surge in the concentrations of greenhouse gases

(GHGs), such as carbon dioxide (CO₂) and methane (CH₄), with atmospheric CO₂ mixing ratios rising from 280 ppm in the pre-industrial era to 423 ppm in 2023 (see NASA report at https://climate.nasa.gov/vital-signs/carbon-dioxide/?intent=121). The rapid increase in GHG concentrations and the resulting greenhouse effect has led to global warming and more frequent extreme events (Hoegh-Guldberg et al., 2019; Thackeray et al., 2022).

In addition to anthropogenic activities, natural processes also significantly impact atmospheric environment through emissions and sinks. For example, emissions from lightning and soils are important sources of NO_r (Lu et al., 2021b; Pérez-Invernón et al., 2023); vegetation emits substantial biogenic VOCs (Wang F. et al., 2021); volcanic activities release large amounts of SO₂ into the atmosphere (Beckett et al., 2022); and wildfires serve as a dual source of air pollutants and GHGs (Burke et al., 2023; Zheng et al., 2023). Furthermore, global terrestrial CO₂ sinks offset approximately 34% of CO₂ emissions from fossil fuel use and land-use changes in 2013-2022 (Friedlingstein et al., 2023). Therefore, accurate assessment of emissions of atmospheric pollutants and GHGs (including sinks) is crucial for understanding their evolution in the atmosphere and their environmental and climate impacts, as well as for policymaking on emission control and sustainability.

The concentrations, emissions and sinks of air pollutants and GHGs can be indirectly inferred through remote sensing with satellite instruments. With the recent rapid advancement in satellite remote sensing instruments and retrieval algorithms, satellite observations have been widely applied to studying the spatiotemporal variations in air pollutants and GHGs, offering unprecedented opportunities for top-down quantification of emissions. The resulting top-down emission data complement traditional bottom-up approaches based on emission inventories and process models, which often face limitations in accuracy, spatiotemporal resolution, and timeliness.

Operational satellite sensors include polar-orbiting instruments, such as the Ozone Monitoring Instrument (OMI; Boersma et al., 2007), TROPOspheric Monitoring Instrument (TROPOMI; van Geffen et al., 2020), Measurement Of Pollution In The Troposphere (MOPITT; Deeter et al., 2003), and Green-house gas Observing Satellite (GOSAT; Butz et al., 2011), as well as geostationary orbit instruments, such as the Geostationary Environmental Monitoring Spectrometer (GEMS; Kim et al., 2020) and Tropospheric Emissions: Monitoring of Pollution (TEMPO; Zoogman et al., 2017).

Over the past decade, China has launched a constella-

tion of advanced satellite sensors, such as the Environment Monitoring Instrument (EMI; Zhang C. X. et al., 2020), Geostationary Interferometric Infrared Sounder (GIIRS; Zeng et al., 2023), Ozone Monitoring Suite (OMS; Wang Q. et al., 2024), Exploratory Satellite for Atmospheric CO₂ (TanSat; Liu et al., 2018), and the world's first active CO₂ remote sensing satellite, i.e., the Atmospheric Environment Monitoring Satellite (DQ-1; Han et al., 2018). These have established China's initial capability for domestic satellite-based atmospheric composition monitoring and emission quantification.

Satellite-based emission inversion for air pollution and GHGs has undergone remarkable advancements over the past two decades. Early studies, which were constrained by inadequate satellite spatial coverage and/or revisit frequency, predominantly focused on emission quantification at coarse spatiotemporal resolutions (Jiang et al., 2017, Miyazaki et al., 2020, Zhang Y. et al., 2021, Qu et al., 2022; Wang H. M. et al., 2022). The advent of highprecision polar-orbiting platforms like TROPOMI in recent years has enabled kilometer-level, daily-scale emission inversions (Kong H. et al., 2022; Li H. et al., 2023; Qin et al., 2023a; Zhang Q. Q. et al., 2023; Tang et al., 2024a), while emerging geostationary satellites are now advancing inversion capabilities with enhanced temporal resolution for diurnal variation (Shu et al., 2022; Watine-Guiu et al., 2023; Hsu et al., 2024). This technological evolution thus positions rapid high-resolution satellitebased emission inversion as a critical frontier in atmospheric research.

From the perspective of emission inversion method, early inversion studies were limited by computational resources, and they relied primarily on simplified approaches, such as three-dimensional variational (3D-Var) methods and local mass balance techniques (Arellano et al., 2004; Fu et al., 2007; Jones et al., 2009; Lamsal et al., 2011; Lin and McElroy, 2011). Driven by advances in computer technology, sophisticated data assimilation systems, including four-dimensional variational (4D-Var) and ensemble Kalman filters, have gained widespread adoption (Jiang et al., 2015; Wang Y. et al., 2020; Jiang F. et al., 2022; He et al., 2023b; Jin et al., 2023). To meet growing demands for high-resolution inversions, computationally efficient methods such as Gaussian models (Beirle et al., 2011; Liu et al., 2016), two-dimensional (2D) divergence models (Beirle et al., 2019; Qin et al., 2023a) and 2D chemical transport models (Kong et al., 2019) have undergone rapid development. Most recently, researchers are actively exploring machine learning techniques (Huang et al., 2021; He T. L. et al., 2022; Li and Xing, 2024) to achieve further breakthroughs in computational efficiency and/or spatiotemporal resolution.

In recent years, a series of advancements in satellite-based inversion, driven by Chinese researchers, has greatly improved our ability to quantify the spatiotemporal patterns and evolution of atmospheric pollutant emissions (Lin and McElroy, 2011; Jin et al., 2023; Qin et al., 2023a; Zuo et al., 2023) and characteristics of GHG sources and sinks (Zheng et al., 2020b; Zhang Y. et al., 2021; He et al., 2023b; Shen et al., 2023). Relevant studies focused on the rapidly evolving global atmospheric conditions (Li et al., 2020, Jiang Z. et al., 2022; Huang et al., 2023) and China's own satellite observation capabilities (Han et al., 2018; Liu et al., 2018; Han et al., 2020; Zhang P. et al., 2021, Su et al., 2022; Zeng et al., 2023), making important contributions to the academic development and environmental governance.

To commemorate the 100th Anniversary of the Chinese Meteorological Society, this review synthesizes two decades of Chinese research achievements in satellite-based emission inversion, based on comprehensive literature survey using targeted keyword combinations (species names + "emission"/"inversion" + "satellite"), complemented by the authors' known literature collection. Our synthesis includes a summary of inversion methodologies, including data assimilation, local mass balance, Gaussian models, 2D models, and machine learning; as well as key findings on emission inversions for NO_r, NH₃, SO₂, CO, formaldehyde (HCHO; a VOC tracer), glyoxal (CHOCHO; ano-ther VOC tracer), CO2 (including sources and sinks), and CH₄. The historical evolution of satellite-based inversion methods and target species, current challenges and future perspectives are further discussed lastly.

2. Emission inversion methodology

As a top-down approach, emission inversion uses atmospheric observations from satellites and other platforms to inversely estimate emissions of air pollutants and GHGs. The methodologies can generally be summarized into two categories. The first category requires a priori emission data (typically provided by bottom-up emission inventories or process models) and three-dimensional chemical transport models, mainly including data assimilation, simplified methods such as local mass balance, as well as machine learning-based methods which are currently in the early development stage. The second category operates without a priori emission data and chemical transport models, by leveraging concentration observations and meteorological data to derive emis-

sions through Gaussian plume models or two-dimensional model approaches. This section provides a summary of the inversion methods.

2.1 Data assimilation

Data assimilation has a wide range of applications in Earth sciences. The various data assimilation methods share a common mathematical foundation, which can be traced back to Bayes' theorem, typically expressed mathematically as:

$$P(\mathbf{x}|\mathbf{y}) = \frac{P(\mathbf{y}|\mathbf{x})P(\mathbf{x})}{P(\mathbf{y})},\tag{1}$$

where P(x|y) represents the a posteriori conditional probability density function to be characterized, P(x) and P(y) are the a priori probability density functions of variables x and y, respectively, and P(y|x) is the likelihood function of variable y given parameter x. The goal of data assimilation is to find the optimal solution of x that maximizes P(x|y) given the available information about y.

In emission inversion, x represents the emissions of pollutants and GHGs to be optimized, and y corresponds to the observed concentrations. For carbon sink inversion, x represents the carbon fluxes. Assuming that all probability density functions are Gaussian distributions, P(x|y) can be expressed as (Rodgers, 2000):

$$\ln P(x|y) = -\frac{1}{2} \left[(F(x) - y)^{T} S_{\Sigma}^{-1} (F(x) - y) + (x - x_{a})^{T} S_{a}^{-1} (x - x_{a}) \right] + c = -\frac{1}{2} J(x) + c. \quad (2)$$

Here, F represents the relationship between x and y, often characterized by atmospheric chemical transport models or other physics-based models with varying complexity; x_a represents the a priori emissions; S_{Σ} and S_a denote the observational error covariance (from uncertainties in measurements and model simulations) and the a priori error covariance, respectively; and J is the cost function. The target of data assimilation is to obtain optimized emission estimates corresponding to the minimized cost function. By setting the gradient of the cost function to zero:

$$\nabla_{x} J(x) = 2\nabla_{x} F^{T} S_{\Sigma}^{-1} (F(x) - y) + 2S_{a}^{-1} (x - x_{a}) = 0.$$
 (3)

The posteriori emissions can be analytically solved as (Rodgers, 2000):

$$\widehat{\boldsymbol{x}} = \boldsymbol{x}_{a} + \left(\nabla_{\boldsymbol{x}} \boldsymbol{F}^{\mathsf{T}} \boldsymbol{S}_{\Sigma}^{-1} \nabla_{\boldsymbol{x}} \boldsymbol{F} + \boldsymbol{S}_{a}^{-1}\right)^{-1} \nabla_{\boldsymbol{x}} \boldsymbol{F}^{\mathsf{T}} \boldsymbol{S}_{\Sigma}^{-1} (\boldsymbol{F}(\boldsymbol{x}_{a}) - \boldsymbol{y}). \tag{4}$$

Based on this analytical approach, a 3D-Var emission inversion method can be constructed. The 3D-Var approach faces significant limitations in large-scale emission inversions, primarily due to difficulties in formulat-

ing the Jacobian matrix ($\nabla_x F$), and its inherent neglect of temporal dependencies (i.e., the temporal differences between emissions and observed concentrations). To overcome these methodological constraints, the 4D-Var method was developed, with its cost function reformulated as (Elbern et al., 2000; Henze et al., 2007):

$$J(x) = \sum_{k=1}^{N} (F_k(x) - y)^{T} S_{\Sigma}^{-1} (F_k(x) - y) + (x - x_a)^{T} S_a^{-1} (x - x_a).$$
 (5)

where k represents the time steps from the start to the end of the assimilation period. The gradient of the cost function can be expressed as:

$$\nabla_{\mathbf{x}}J(\mathbf{x}) = \sum_{k=1}^{N} \left[2S_{\Sigma}^{-1} \left(\mathbf{F}_{k}(\mathbf{x}) - \mathbf{y} \right) \frac{\partial \mathbf{F}_{k}}{\partial \mathbf{x}} \right] + 2S_{\mathbf{a}}^{-1} \left(\mathbf{x} - \mathbf{x}_{\mathbf{a}} \right). \quad (6)$$

Unlike the analytical solution, the 4D-Var method does not require an explicit construction of Jacobian matrices and calculates the sensitivity of concentrations to emissions through backward simulation (adjoint modeling), where *I* represents an unit matrix:

$$\frac{\partial \mathbf{F}_k}{\partial \mathbf{x}} = \mathbf{I} + \frac{\partial \mathbf{F}_k}{\partial \mathbf{F}_{k-1}} \frac{\partial \mathbf{F}_{k-1}}{\partial \mathbf{x}}.$$
 (7)

A series of methodological innovations in variational approaches have been conducted by Chinese researchers. For example, Kong et al. (2019) developed a 2D atmospheric chemistry transport model (PHLET) and its adjoint model, achieving fast, kilometer-scale resolution emission inversion; and Tang et al. (2023) extended the widely used GEOS-Chem adjoint model by adding support for multiple meteorological datasets and prior emission data, for better assessing prior data-induced errors in emission inversion.

The 4D-Var method often requires adjoint models of 3D chemical transport models, which can be challenging to develop and maintain. To address this issue, ensemble methods have been used to quantify uncertainties, motivating the application of ensemble Kalman filters. The cost function in ensemble Kalman filters is formulated as (Hunt et al., 2007; Miyazaki et al., 2012):

$$J(w) = \left[F(\overline{x}^b + X^b w) - y \right]^{\mathrm{T}} S_{\Sigma}^{-1} \left[F(\overline{x}^b + X^b w) - y \right] + (k-1) w^{\mathrm{T}} w.$$
 (8)

Here, w represents a Gaussian random perturbation vector with a mean of 0 and an ensemble size of k, i.e., we assume that the a priori ensemble members are randomly sampled around the true model state x. The matrix X^b indicates the spread of the a priori ensemble mem-

bers. The optimized a posteriori emissions are also obtained by setting the gradient of the cost function to zero.

In contrast to 4D-Var, which calculates the sensitivity of concentrations to emissions through backward simulation, the ensemble Kalman filter establishes the relationship between concentrations and emissions through perturbing the a priori emissions; thus, the accuracy is influenced by the size of the perturbation ensemble. Additionally, the sensitivity of concentrations to emissions in remote regions over long distances may result in unphysical spatial correlations. Thus the spatial range of correlations is often constrained in practical applications. The inversion results from ensemble Kalman filters thus predominantly reflect (quasi-) local-scale discrepancies between model simulations and observational data, with limited consideration of the long-range transport of air pollutants and GHGs.

2.2 Local mass balance approach

Data assimilation's inherent limitations, stemming from complex inversion frameworks and intensive computational requirements, have motivated the advancement of simplified approaches. The local mass balance approach is frequently applied to the emission inversion of short-lived atmospheric pollutants. Given their short atmospheric lifetimes, inter-grid transport becomes negligible under coarse spatial resolution, and thus only the (local) mass balance within each grid box needs to be considered. The estimation of emissions can be simplified as (Martin et al., 2003; Lin and McElroy, 2011):

$$\frac{E}{E_{\rm a}} = \frac{\Omega}{\Omega_{\rm a}},$$

or

$$\frac{\Delta E}{E_a} = \beta \times \frac{\Delta \Omega}{\Omega_a},\tag{9}$$

where E_a represents the a priori emissions in the grid box, Ω_a refers to the column concentrations simulated by model and the a priori emissions, E is the a posteriori emissions, Ω denotes the satellite-observed column concentration, $\Delta\Omega$ represents the difference between observed and simulated column concentrations, β represents the model-based sensitivity of grid-specific column concentration to emission changes, and ΔE represents the optimized adjustment made to the a priori emissions.

2.3 The Gaussian model and the 2D divergence model

Gaussian models are broadly applied in the inversion of pollutant and GHG emissions from isolated point sources (e.g., power plants and factories) or quasi-point sources (e.g., cities). These methods are independent of chemical transport models and use Gaussian models to fit the distribution of observed concentrations (*M*) in regions downwind of point sources, combining wind information from meteorological assimilation datasets (Beirle et al., 2011; Liu et al., 2016):

$$M(x) = E \times (e \otimes G)(x) + B,$$

$$e(x) = exp\left(-\frac{x - X}{x_0}\right),$$

$$G(x) = \frac{1}{\sqrt{2\pi\sigma}} exp\left(-\frac{x^2}{2\sigma^2}\right).$$
(10)

Here, E represents the point source emission rate, e(x) represents the transport and chemical decay of pollutants and GHGs driven by the wind fields, x denotes the position downwind of the point source, X is the position of the point source, x_0 is the e-folding decay distance that depends on wind speed and the lifetime of chemical species of interest, B represents the background concentration in the region, G(x) stands for atmospheric diffusion to be convolved with the exponential term, and σ represents the standard deviation as well as the spatial smoothing parameter.

The 2D divergence model is another approach for emission inversion that does not require chemical transport models. The general idea of the divergence model is to balance local emissions, horizontal transport, and sinks on a daily basis (Beirle et al., 2019; Qin et al., 2023a):

$$E = \nabla \cdot (CV) + \frac{C}{\tau}.\tag{11}$$

where E stands for the emissions of chemical species, C represents the observed concentrations, V is the horizontal wind vector, and τ represents the atmospheric lifetime of the chemical species. Atmospheric transport is parameterized by horizontal divergence of the flux (CV)of chemical species, where divergence and convergence stand for outward and inward transport, respectively. The divergence model often assumes that the atmospheric lifetimes are constant in time and space. As a result, the quality of emission inversion via the divergence model can vary significantly over different regions and time periods, especially for chemically active and highly nonlinear atmospheric constituents (e.g., NO_r). For instance, under certain conditions, the divergence model can lead to negative emissions, which reflect a major limitation of the approach. Efforts have been made to improve the 2D divergence model. For example, Qin et al. (2023a) considered temporal variations and flexibly fitted the parameters of the first-order chemical decay and transport terms to better estimate the impact of local chemical transport processes.

2.4 Machine learning

The complexity of physics-based data assimilation frameworks and their high computational cost pose significant barriers for practical applications. Nevertheless, application of data-driven machine learning, particularly neural network methods, is rapidly expanding in atmospheric environmental research. Mathematically, the training process of neural networks can be regarded as multivariate nonlinear regression, aiming to "learn" any nonlinear multidimensional function (LeCun et al., 2015; Goodfellow et al., 2016). Like the ensemble Kalman filters, the machine learning-based inversions use atmospheric chemical transport model simulations as the ground truth in the training process to establish a relationship function between concentrations and emissions. Compared with traditional data assimilation methods, pretrained models can be used to estimate emissions, which require dramatically reduced computational resources. The application of machine learning in emission inversions is still in the early development stage (Huang et al., 2021, He T. L. et al., 2022, Li and Xing, 2024).

From the perspective of statistics, the goal of training processes of neural networks is to optimize the parameters of interconnected units (often referred to as neurons) to directly represent the a posteriori probability density function. Each neuron has two learnable parameters: the weight (w) and the bias (b). A neuron receives inputs from all neurons in the previous layer and broadcasts an activated output to the next layer. For a neuron k in the output layer, we can derive:

$$z_k = \sum_j a_j w_{jk} + b_k, \tag{12}$$

$$a_k = g_k(z_k), \tag{13}$$

where w_{jk} represents the weight applied to the output of neuron j in the previous hidden layer, while b_k denotes the bias adjustment applied to neuron k. z_k is the propagation equation, which sums over the weighted outputs of all neurons in the previous layer. g_k is referred to as the activation function, which performs a nonlinear transformation on the propagated signal.

Before the training begins, the neural networks are randomly initialized and the initial prediction differs significantly from the ground truth. Similar to data assimilation methods, a cost function can be defined as:

$$J(a_k - t_k) = (a_k - t_k)^2 / 2,$$
 (14)

where t_k stands for the ground truth and a_k is the prediction made by neural networks. The gradients of the cost

function with respect to the weights and biases of each neuron in the last layer can be expressed as:

$$\frac{\partial J}{\partial w_{jk}} = (a_k - t_k) g'_k(z_k) a_j. \tag{15}$$

$$\frac{\partial J}{\partial \boldsymbol{b}_k} = (\boldsymbol{a}_k - \boldsymbol{t}_k) \, \boldsymbol{g}_k'(\boldsymbol{z}_k). \tag{16}$$

By setting the gradient to zero, we can backpropagate and optimize the weights and biases of all the neurons in the previous hidden layer connected to neuron *k*. Similar to the 4D-Var method, the training process is performed iteratively until the cost function reaches the minimum.

3. Atmospheric pollutant emission inversion

In Section 2, we introduced the main emission inversion methods. This section will summarize the emission results of atmospheric pollutants obtained by using different inversion approaches. Satellite-based inversion of atmospheric pollutant emissions has predominantly targeted gaseous species associated with PM_{2.5} and O₃ formation, including NO_x, NH₃, HCHO, CHOCHO, SO₂ and CO, depending on the detectability of atmospheric constituents through current remote sensing technologies. While atmospheric PM_{2.5} originates from both direct emissions and secondary chemical production from gaseous precursors, the predominance of the latter pathway has limited scholarly efforts in direct PM_{2.5} emission inversion via satellite remote sensing; therefore, we do not include such studies here.

3.1 Nitrogen oxides

Nitrogen oxides ($NO_x = NO + NO_2$) are major air pollutants emitted from both natural and anthropogenic sources, such as fossil fuel combustion, biomass burning, soil emissions, and lightning activity. NO_x directly impacts human health, and also contributes to the O_3 production via photochemical reactions with VOCs as well as the formation of nitrate and sulfate $PM_{2.5}$. The atmospheric lifetime of NO_x ranges from a few hours to tens of hours, with a large seasonal variability (shorter in summer, longer in winter). NO_x is primarily removed through dry and wet deposition of its oxidation products (nitric acid and nitrate), which leads to acid deposition that causes soil acidification, compromises agricultural productivity, and corrodes infrastructure.

Satellite-based UV/Vis spectrometers enable global NO₂ column retrievals. Commonly used satellite instruments include polar-orbiting sensors such as the Global Ozone Monitoring Experiment (GOME, Martin et al.

(2002)), OMI (Boersma et al., 2007), TROPOMI (van Geffen et al., 2020), and China's EMI (Zhang C. X. et al., 2020) and OMS (Wang Q. et al., 2024), as well as geostationary instruments such as GEMS (Kim et al., 2020) and TEMPO (Zoogman et al., 2017). These satellite observations are widely applied to study the lifetime of NO_2 and its spatial variability (Zhang et al., 2007; Duncan et al., 2016; Jiang et al., 2018) and to derive NO_x emissions using various inversion methods (Lamsal et al., 2011; Miyazaki et al., 2020).

Continuous progress have been made in satellite-based NO_x emission inversions. Given the short lifetime of NO_x , inversion studies on NO_x often employ the local mass balance method, which neglects the influence of regional transport on NO₂ column concentrations. As such, the mass balance method is more suitable for emission inversions with relatively low spatial resolutions ranging from tens to hundreds of kilometers (Lin and McElroy, 2011, Lin, 2012, Lin et al., 2015, Chen Y. F. et al., 2021, Zhu et al., 2021; Li H. et al., 2024). The mass balance method has also been explored and applied to regional high-resolution NO_x emission inversions (Yang et al., 2019; Yang Y. et al., 2021). Combining observations from multiple satellite instruments instead of relying on a single source can effectively increase the amount of observational information (Lin et al., 2010; Gu et al., 2014). The nonlinear response of NO₂ column concentrations to NO_x emissions (Gu et al., 2016) and the discrepancies in satellite observations (Yang et al., 2019) have important influences on NO_x emission inversions. By taking advantage of the rapid inversion by use of the mass balance method, extensive assessments have been conducted on the impact of the COVID-19 lockdown on NO_x emissions from various perspectives (Zhang R. X. et al., 2020, Zhu Y. Z. et al., 2022, Liu et al., 2023).

In addition to the local mass balance, Gaussian models and their variants, operationally independent of chemical transport models, have also been widely utilized. These methods are well suited for the rapid assessment of point source emissions and are frequently applied to NO_x emission inversions for power plants and cities (by treating cities as point sources). The availability of newergeneration observation platforms, such as TROPOMI and GEMS, has further promoted their applications (Zhang et al., 2015, Liu et al., 2016; Liu F. et al., 2017; Li Y. S. et al., 2018; Xue et al., 2022; Luo et al., 2023; Tang et al., 2024a, b; Xu et al., 2024).

Advanced and innovative inversion algorithms have continually been developed to achieve fast, fine-scale, and reliable NO_x emission inversion. Kong et al. (2019) established a 2D atmospheric chemical transport model (PHLET, 0.05° × 0.05° resolution) with adjoint capabilities, overcoming the limitations of foreign-developed fast inversion methods such as Gaussian and 2D divergence models in characterizing complex emission sources and/ or local nonlinear chemical transport processes. With PHLET, they achieved OMI-based quantification of summertime NO_x emissions over the Yangtze River Delta during 2012-2015 (Fig. 1). Kong H. et al. (2022) further enhanced this method to constrain NO_x emissions for summer 2019 in the whole Chinese mainland with TRO-POMI data, and they revealed numerous small-tomedium emission sources omitted in conventional bottom-up inventories. Building on this foundation, Kong et al. (2023) further quantified NO_x emissions over the Qinghai-Xizang Plateau during summer, and discovered previously unknown high-intensity NO_x sources from remote plateau lakes, which were linked to microbial processes under climate warming. Building on divergence model approach, Qin et al. (2023a) improved the characterization of local chemical transport processes through parameter fitting of first-order chemical decay and transport terms. Their new method produced a daily 0.05° × 0.05° resolution NO_x emission dataset for China's Energy Golden Triangle region in 2019. This method was subsequently applied by Li X. L. et al. (2023) and Liu et al. (2024) to estimate NO_x emissions in Shanxi, China and to quantify NO_x emissions from biomass burning and rapid urbanization in Southeast Asia. Pan et al. (2023) developed a NO_x emission dataset in China in 2019 at 1×1 km resolution by using the divergence model and TROPOMI data, and they revealed over 100 super-emitters (primarily factories) missing from existing emission inventories.

Through systematic comparison of three fast inver-

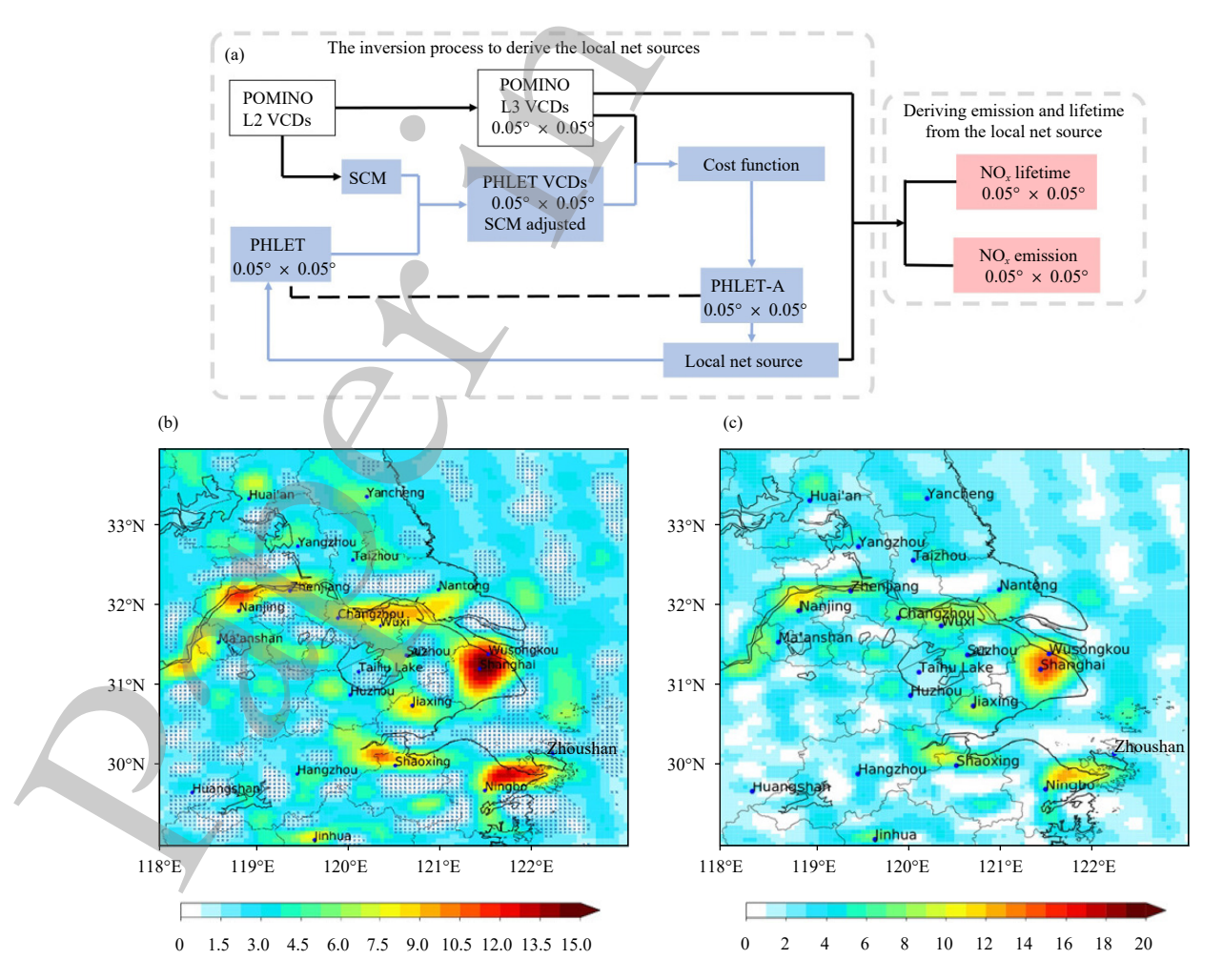


Fig. 1. Atmospheric NO_x emission (kg km⁻² h⁻¹) inversion based on the two-dimensional (2D) atmospheric chemical transport model (PHLET) and its adjoint. (a) Schematic diagram of the inversion algorithm. (b) Total a posteriori NO_x emissions in the Yangtze River Delta during summer 2012–2015. The blue crosses indicate where the relative errors exceed 100%. (c) A posteriori NO_x emissions from the anthropogenic sources. Cited from Kong et al. (2019).

sion approaches (Gaussian, PHLET, and divergence models) in NO_x emission estimates for the North China Plain, Wang S. J. et al. (2024) found that Gaussian model is primarily suited for point source emissions but performs poorly in regions with densely distributed emission sources; the divergence model can quickly identify major emission source locations but suffers from issues such as underestimation and negative emissions; and PHLET explicitly accounts for atmospheric transport and nonlinear chemical processes, yielding results that align well with independent datasets for road network and population distribution.

The application of machine learning to NO_x emission inversion has also been actively explored. Using WRF-CMAQ simulation datasets, Xing et al. (2022) developed machine learning models to inversely derive NO_x emissions from OMI observations in 2017 in China, demonstrating computational efficiency gains compared to conventional approaches. Li and Xing (2024) developed a NO_2 concentration dataset for China in 2017–2021, based on the WRF-CMAQ simulation and OMI observations, and estimated NO_x emissions with the developed NO_2 dataset. They found that NO_x emissions were higher in winter, but wintertime NO_x emissions decreased by 40% in 2020, attributed to emission decline associated with the COVID-19 and environmental regulations.

3.2 Ammonia

Ammonia (NH₃) is the most abundant alkaline gas in the atmosphere. Its heterogeneous reactions with SO₂ and NO_x lead to the formation of ammonium nitrate and ammonium sulfate. NH₃ in the atmosphere is emitted primarily from two anthropogenic sources: agricultural fertilization and livestock waste (Li et al., 2021). Observational data reveal that regions with intensive agricultural activities and high livestock densities, such as India and the North China Plain, are global hotspots of atmospheric NH₃ concentrations. Accurately quantifying the spatiotemporal distribution of NH₃ emissions is of critical scientific and practical importance for atmospheric environmental research and nitrogen management at both the country and global scales.

Satellite remote sensing serves as the primary approach for global atmospheric NH₃ monitoring. Commonly used satellite instruments include Tropospheric Emission Spectrometer (TES; Beer et al., 2008), Atmospheric Infrared Sounder (AIRS; Warner et al., 2016), Infrared Atmospheric Sounding Interferometer (IASI; Clarisse et al., 2009), Cross-track Infrared Sounder (CrIS; Shephard and Cady-Pereira, 2015), and China's GIIRS (Zeng et al., 2023). The associated satellite data-

sets are applied to monitor the spatiotemporal variability of atmospheric NH₃ concentrations (Ge et al., 2020, Deng et al., 2021), and are combined with atmospheric chemical models and data assimilation techniques to derive NH₃ emissions (Sitwell et al., 2022).

Data assimilation methods are often employed to conduct satellite-based atmospheric NH₃ emission inversion. For example, Zhu et al. (2013) and Zhang et al. (2018) integrated the GEOS-Chem adjoint model and TES observations to estimate NH₃ emissions in the United States and China. Jin et al. (2023) developed a 4D ensemble variational (4DEnVar) data assimilation system based on the GEOS-Chem model, achieving high-efficiency NH₃ emission inversion with localized analysis techniques. A top-down estimate of NH₃ emissions in China was obtained in Jin et al. (2023), revealing severe underestimations (approximately 50% assimilation increments) in the MEIC inventory over North, East, and Northwest China.

In addition to data assimilation, local mass balance methods have been explored for NH₃ emission inversions (Chen et al., 2023, Wen et al., 2024). Luo et al. (2022) established a linear model linking NH₃ emissions to concentrations through atmospheric simulations, generating a global monthly NH₃ emission dataset at $4^{\circ} \times 5^{\circ}$ resolution (2008–2018) using IASI observations. Liu et al. (2022a) synergized IASI/GIIRS observations with GEOS-Chem simulations to perform a rapid estimation of NH₃ emissions over 2008–2019 in China. Liu et al. (2022b) constrained livestock NH₃ emissions in Hebei, China using IASI observations, revealing a 5.8% annual growth in 2008–2020 as well as seasonality (higher in spring and summer) in NH₃ emissions. Furthermore, the Gaussian model method was also successfully implemented for NH₃ emission inversion—for example, Xie et al. (2024) quantified warm-season (May-September) NH₃ emissions and atmospheric lifetimes in Urumqi and Golmud (2008–2023) using IASI observations, providing critical insights into urban NH3 emissions across western China.

3.3 Volatile organic compounds

Formaldehyde (HCHO) and glyoxal (CHOCHO), detectable by satellite instruments, serve as proxies for tracking VOC emissions. HCHO predominantly originates from secondary oxidation of biogenic or anthropogenic VOCs and combustion of organic matter; and CHOCHO is produced from less amount of VOC species with lower yield. With atmospheric lifetimes of a few hours, HCHO and CHOCHO undergo rapid removal via OH-driven oxidation, photolysis, and deposition processes, making them reliable indicators of regional VOC

emissions, as well as proxies for quantifying VOC emissions. Current spaceborne capabilities for HCHO/CHOCHO monitoring include OMI (González Abad et al., 2015), TROPOMI (De Smedt et al., 2018), Ozone Mapping and Profiler Suite (OMPS, Nowlan et al. (2023)), GEMS (Kwon et al., 2019), TEMPO (Zoogman et al., 2017), and China's EMI (Su et al., 2022). These satellite datasets are extensively applied to assess the spatiotemporal distributions of VOCs (Chen et al., 2019), anthropogenic emissions (Sun et al., 2021; Pu et al., 2024), and the formation of tropospheric O₃ pollution (Wang W. N. et al., 2021; Ren et al., 2022).

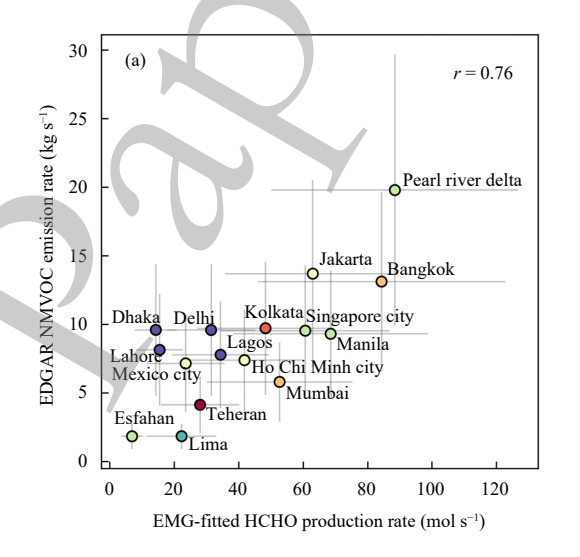
VOC emission inversion studies have largely taken advantage of the nearly linear relationship between VOC emissions and HCHO and CHOCHO concentrations. Early research by Fu et al. (2007) constrained biogenic, anthropogenic, and biomass burning VOC emissions across Asia through linear regression techniques combining GEOS-Chem simulations with HCHO column retrievals; and Zhu et al. (2014) analyzed summertime HCHO enhancements (2005-2008) in OMI-observed downwind plumes relative to regional baselines. Recently, Wang F. et al. (2021) implemented local mass balance approaches with TROPOMI data to constrain VOC emissions in eastern China; Li W. et al. (2023) implemented local mass balance approaches with TRO-POMI data to resolve VOC and NO_x emissions in Qinghai Province; and Feng et al. (2024) revealed 50% overestimations in a priori VOC emission inventories in China in summer 2022 through ensemble Kalman filter assimilation of TROPOMI observations.

In recent years, there has been a growing focus on estimating point source emissions of VOCs. For example,

Zuo et al. (2023) identified global HCHO point sources using TROPOMI observations. They aligned the observed HCHO plumes with wind fields and employed a Gaussian model to fit HCHO concentrations along downwind plumes. This approach allowed the estimation of the production rates of HCHO from point sources relative to background levelss (Fig. 2), demonstrating a strong correlation with VOC emissions from the EDGAR inventory (r = 0.76). The joint analysis of HCHO and CHOCHO observations offers unique advantages for VOC source attribution, given their differential yields across VOC precursors. This multi-species strategy is exemplified by Cao et al. (2018): By assimilating both HCHO and CHOCHO retrievals into GEOS-Chem adjoint framework, they uncovered stronger seasonal variability in VOC emissions in China than inventory estimates, highlighting the necessity of joint assimilation of HCHO and CHOCHO observations to distinguish VOC species and to better constrain anthropogenic sources.

3.4 Sulfur dioxide

Sulfur dioxide (SO₂) in the atmosphere is emitted mainly by the combustion of fossil fuel and the processing of sulfur-containing raw materials. Volcanic eruptions can also release substantial amounts of SO₂ into the atmosphere. Atmospheric SO₂ poses threats to human health and, through oxidation to sulfate aerosols, impacts global environmental and climate systems. Satellite instruments play a key role in monitoring atmospheric SO₂. Commonly used sensors include OMI (Theys et al., 2015), OMPS (Yang et al., 2013; Li C. et al., 2024), TROPOMI (Theys et al., 2017), China's EMI (Xia et al., 2021) and OMS (Wang Q. et al., 2024) on polar orbiting satellites, as well as GEMS (Kim et al., 2020) and



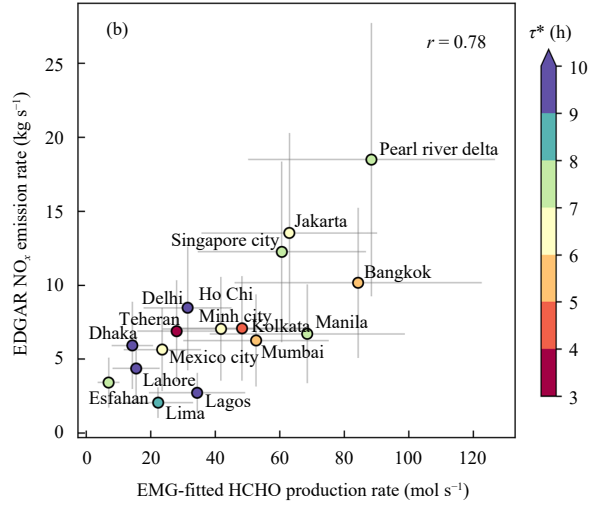


Fig. 2. Comparison between EMG-fitted effective HCHO production rates with total anthropogenic (a) non-methane VOC and (b) NO_x from EDGAR inventory. Cited from Zuo et al. (2023).

TEMPO (Zoogman et al., 2017) in geostationary orbit. Extensive SO_2 observations are vital for understanding the spatiotemporal distribution of SO_2 (Wei et al., 2023), improving the parameterization schemes of SO_2 model simulations, and estimating SO_2 emissions (Hu et al., 2022; Weismann et al., 2023).

Gaussian models or other plume methods are often employed to estimate SO_2 point source emissions based on satellite observation data. For instance, Wang et al. (2015) employed OMI SO_2 observations with a refined 2D Gaussian fitting method to quantify emission reduction before and after the implementation of flue gas desulfurization (FGD) facilities at 26 coal-fired power plants in China. Their results revealed an average SO_2 emission reduction of $56\% \pm 21\%$ between 2005 and 2010 due to FGD adoption. Cai et al. (2022) estimated SO_2 emissions from the 2019 Raikoke volcanic eruption to be about 2.1 Tg by integrating AIRS and TROPOMI satellite data.

SO₂ emissions can also be constrained with the 4D-Var method by assimilating satellite observations. For example, Wang et al. (2016) inverted anthropogenic SO₂ emissions by assimilating OMI observations into the GEOS-Chem adjoint model, and estimated the impact of emission control measures during the 2008 Beijing Olympics. They reported an approximate 20% decline in SO₂ emissions during the event and demonstrated that a posteriori emission estimates significantly improved model accuracy in simulating near-surface concentrations and vertical column densities of SO₂. In addition, local mass balance methods have been successfully applied for SO₂ emission inversion. Li M. et al. (2018) estimated SO₂ and NO_x emissions in China for 2005 and 2010 using OMI data, revealing that a priori emission inventories underestimated SO₂ emissions. They attributed this underestimation to inaccurate estimates of civil bulk coal emissions.

3.5 Carbon monoxide

Carbon monoxide (CO) is a primary air pollutant generated during incomplete combustion and the oxidation of VOCs in the atmosphere, and it is primarily removed through oxidation by OH. CO can produce O₃ through photochemical reactions, thereby having a significant impact on global OH levels and the oxidative capacity of the atmosphere. With a tropospheric lifetime of roughly two to three months, CO can be transported regionally or even intercontinentally, making it a widely used tracer for studying air pollutant transport. CO concentrations in the atmosphere can be measured by satellite-based remote sensing instruments, including the SCanning Ima-

ging Absorption SpectroMeter for Atmospheric CHartography (SCIAMACHY; Bogumil et al., 2003), AIRS (McMillan et al., 2005), IASI (George et al., 2009), MO-PITT (Deeter et al., 2003), and TROPOMI (Landgraf et al., 2016). These observations are widely used to investigate the lifetime of CO and its spatiotemporal variations (Liu et al., 2013; Hedelius et al., 2021), and inversions of CO emissions (Jiang et al., 2011; Miyazaki et al., 2020).

As early as 2007, Lin et al. (2007) inverted global atmospheric CO emissions using the MOZART model and MOPITT observations. Recent studies have increasingly employed data assimilation methods. For instance, Jiang et al. (2017) developed a dual-step inversion method combining Kalman filtering and 4D-Var to eliminate model biases related to long-range transport. By assimilating MOPITT observations, they inferred global CO emissions during 2001–2015. Zheng et al. (2018) used a 4D-Var method based on the LMDZ-INCA model to assimilate MOPITT data for East Asia for 2005-2016, revealing that a priori inventories underestimated the decline rate of CO emissions in China. Tang et al. (2023) extended the widely used GEOS-Chem adjoint model (4D-Var) by adding support for updated meteorological datasets and emission inventories. Using this upgraded framework, their subsequent studies assimilated MO-PITT observations to derive global atmospheric CO emissions for 2003-2022, revealing that anthropogenic emission reductions drove CO declines at mid-low latitudes in the Northern Hemisphere, while wildfires elevated CO levels at high latitudes.

Furthermore, Gaussian models have been tried by Chinese researchers for rapid monitoring and quantification of CO point-source emissions. For example, Tian et al. (2022a) combined a Gaussian model with TROPOMI observations to estimate CO emissions from four industrial point sources in China and India. Tian et al. (2022b) subsequently applied this method to quantify CO emissions from 14 Chinese industrial point sources, finding that most sources exceeded inventory estimates.

4. Inversion of GHG sources and sinks

Current satellite instruments can effectively monitor changes in CO₂ and CH₄ concentrations in the atmosphere, enabling inversions of corresponding emissions and carbon sinks. However, constrained by technical limits, there are currently no satellite observations of nitrous oxide (N₂O), an important greenhouse gas. Building upon the emission inversion methods introduced in Section 2, this section provides a review of the inversion res-

ults on CO₂ and CH₄.

4.1 Carbon dioxide emissions

Carbon dioxide (CO₂) is the most important anthropogenic GHG, with its global mean atmospheric mixing ratio surging from 280 ppm during the pre-industrial era to 423 ppm in 2023. Anthropogenic activities dominate CO₂ emissions, where fossil fuel combustion and landuse changes contribute approximately 88.1% and 11.9%, respectively (Friedlingstein et al., 2023). Since the beginning of the 21st century, infrared satellite remote sensing has driven rapid advancements in monitoring global column-averaged CO₂ mixing ratios (XCO₂). Key spaceborne instruments include GOSAT (Butz et al., 2011) and GOSAT-2 (Suto et al., 2021), those used in the Orbiting Carbon Observatory missions (OCO-2 and OCO-3; Crisp et al., 2017; Eldering et al., 2019), as well as China's TanSat (Liu et al., 2018; Hong et al., 2022) and DQ-1 (the world's first active carbon monitoring satellite; Han et al., 2018). These observations are widely used to characterize the spatiotemporal distribution and underlying mechanisms of atmospheric CO₂ (Bai et al., 2010; He et al., 2020), providing critical data support for satellite-based emission inversions (Wu et al., 2020; Nassar et al., 2021).

Nonetheless, the long atmospheric lifetime of CO₂ (at least several decades) combined with its elevated background concentration results in weak enhancement signals from anthropogenic emissions (typically < 5 ppm). The enhancement signals are often comparable to satellite observation uncertainties (Nassar et al., 2017; Reuter et al., 2019), posing significant challenges for direct emission inversions. Recent progress in satellite sensor technology and the emergence of advanced inversion algorithms enable multi-scale CO₂ emission estimation.

Satellite-based CO₂ emission inversion methods include data-driven and model-driven approaches. The data-driven method integrates satellite-derived XCO₂ data with local wind field information under steady-state assumptions to estimate emissions from large point sources and isolated cities (Hu et al., 2021; Guo et al., 2023; Lin et al., 2023). For example, Wang Y. et al. (2019) developed a plume monitoring inversion framework to quantitatively characterize city-level and pointsource CO₂ emissions and associated uncertainties (Wang Y. L. et al., 2020). Employing OCO-2 observations in 2014–2019, Zheng et al. (2020a) applied a Gaussian plume model to correlate XCO₂ enhancement signals with adjacent anthropogenic sources, quantifying CO₂ emissions from 60 plume cases across 46 Chinese cities. Their results revealed an annual total emission of 1.3 Gt, which accounted for 13% of China's total and showed better consistency with the domestic MEIC inventory than global inventories (EDGAR, ODIAC).

Model-driven approaches typically employ 3D Eulerian models (e.g., meteorology-chemistry online coupled model, WRF-Chem), Lagrangian models (e.g., time-reversed Lagrangian particle dispersion model X-STILT and coupled meteorology-particle dispersion model WRF-FLEXPART). Yang et al. (2017) inverted CO₂ emissions in China in 2012 using GOSAT satellite data combined with an ensemble Kalman filter. He et al. (2024) compared three inversion methodologies, including the data-driven Gaussian plume model and two maximum likelihood approaches implemented with WRF-Chem and WRF-FLEXPART, respectively. Based on OCO-2 observations in 2014–2021, they estimated CO₂ emissions for 10 power plants in China and 13 power plants in the United States, demonstrating the limited applicability of Gaussian plume models in complex wind field environments. Furthermore, machine learning methods have also been implemented to perform CO₂ emission inversion; for example, Zhang S. Q. et al. (2023) developed a machine learning model integrating multisatellite XCO₂ observations and geographical data to assess anthropogenic CO₂ emissions across China.

Given the limitations of carbon satellites in terms of data volume, quality, and weak XCO₂ enhancement signals, researchers have explored the use of co-emitted air pollutants (CO, NO_x, etc.) as tracers to develop integrated carbon-pollutant inversion techniques. For example, Zheng et al. (2021) inverted CO and CO₂ emissions using MOPITT observations and analyzed wildfire impacts on global carbon emissions; and Zheng et al. (2023) further quantified boreal wildfires' contribution to global emissions, revealing that Northern Hemisphere high-latitude wildfires accounted for 23% of global biomass burning emissions in 2021.

Compared to CO_2 , NO_x exhibits a much shorter atmospheric lifetime (hours) and higher satellite measurement coverage (for NO_2), enabling much better detection of local anthropogenic emission signals to facilitate source-concentration relationship modeling for CO_2 estimation. Zhang Q. Q. et al. (2023) employed a stacked-column model to infer NO_x emissions in Wuhan based on satellite NO_2 observations, and then estimated CO_2 emissions using inventory-based CO_2/NO_x ratios. They detected significant emission reductions in early 2020 that aligned with COVID-19 lockdown measures. Zheng et al. (2020b) developed a joint carbon-pollutant emission inversion system for daily anthropogenic emissions, by integrating near real-time satellite NO_2 observations, a

chemical transport model, and emission inventories at 25 km resolution (Fig. 3). They revealed dramatic anthropogenic CO₂ emission declines during China's pandemic lockdowns; and their subsequent studies further achieved long-term monitoring and inversions for anthropogenic carbon–pollutant emissions (Li H. et al., 2023).

4.2 Carbon dioxide sinks

Terrestrial ecosystems absorb atmospheric CO₂ through photosynthesis while releasing CO₂ through respiration, with the net flux manifested as a carbon sink that plays a vital role in slowing the rise of atmospheric CO₂ concentrations and mitigating global warming. The 2023 global carbon budget report (Friedlingstein et al., 2023) shows that terrestrial ecosystems served as a global carbon sink of $3.3 \pm 0.8 \text{ PgC yr}^{-1}$ in 2013–2022, offsetting approximately 34% of global fossil fuel CO₂ emissions. Moreover, terrestrial carbon sinks exhibit pronounced spatiotemporal variations driven by climate change, nitrogen deposition, and the CO₂ fertilization effect, constituting a primary driver of seasonal and interannual fluctuations in global atmospheric CO₂ concentrations (Le Quéré et al., 2013). Accurate quantification of terrestrial carbon sinks and their spatiotemporal variability therefore has significant scientific importance. The deployment of Chinese and international carbon-monitoring satellites including GOSAT, OCO-2, and TanSat has provided valuable observational data for inverting terrestrial carbon sinks. It has been demonstrated that satellite-based XCO₂ data significantly enhance regional-scale estimates of terrestrial carbon sinks (Deng et al., 2014; Wang H. et al., 2019; Wang H. M. et al., 2022), by reducing uncertainties in carbon sink estimates, enabling quantitative assessments of extreme climate impacts on carbon sinks (Liu J. J. et al., 2017; Wang J. et al., 2022; He et al., 2023a), and improving understanding of climate change effects on terrestrial carbon sinks.

Significant progress has been made in satellite-based terrestrial carbon sink inversions. Yang D. et al. (2021) and Wang H. M. et al. (2022) conducted inversions of global and regional carbon sinks using XCO2 products from the domestically developed TanSat satellite. With their self-developed Glo-bal Carbon Assimilation System version 2 (GCASv2), Jiang F. et al. (2022) assimilated GOSAT XCO₂ observations to produce a dataset (1° resolution) of monthly global terrestrial carbon sink for 2010-2019. Kong Y. et al. (2022) assimilated OCO-2 XCO₂ observations with the THU system, which is based on the GEOS-Chem model and ensemble Kalman filters, to estimate terrestrial carbon sinks on global and regional scales. Employing the independently developed GONGGA system, Jin et al. (2024) constructed a global terrestrial ecosystem carbon flux dataset for 2015-2022 by assimilating OCO-2 XCO₂ data. Li J. et al. (2024) conducted inversions of global carbon sinks in 2019-2021 using OCO-2 XCO₂ and surface CO₂ observations. Furthermore, the GCASv2, GON-GGA, and THU systems were collectively incorporated into the Global

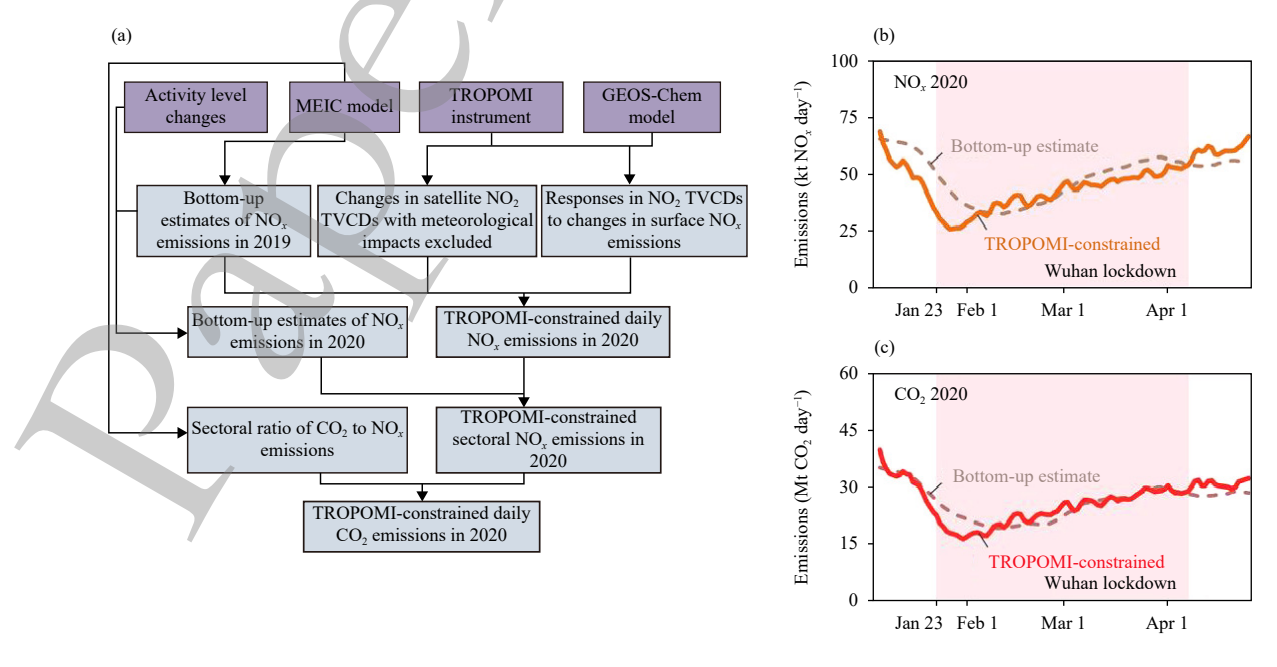


Fig. 3. Anthropogenic carbon-pollutant daily emission joint inversion by integrating satellite remote sensing NO₂ observations and atmospheric chemical transport models. (a) Schematic diagram of the inversion system. (b) A posteriori NO_x emissions in China during early 2020. (c) A posteriori CO₂ emissions in China during early 2020. Cited from Zheng et al. (2020b).

Carbon Project in 2023, demonstrating China's growing contribution and leadership in inversion-based global carbon budget estimation (Friedlingstein et al., 2023).

Regarding regional terrestrial carbon sinks and their variability, He et al. (2023b) estimated that China's terrestrial carbon sink ranged between 0.34 PgC yr⁻¹ (GCASv2) and 0.47 ± 0.16 PgC yr⁻¹ (median \pm standard deviation; OCO-2 v10 MIP) in 2015-2019. They identified southern China as the region with the strongest annual carbon sink (Fig. 4), while peak carbon sink periods during the growing season occurred in Northeast China and other major agricultural zones. Kou et al. (2023) estimated China's 2016 terrestrial carbon sink to be 0.47 PgC yr⁻¹ using GOSAT XCO₂ observations. Wang J. et al. (2022) analyzed global terrestrial carbon sink based on the assimilation of GOSAT observations, and clarified for the first time the impacts of the 2019 positive Indian Ocean Dipole event on terrestrial carbon sinks across the Indian Ocean. Their study revealed that this event severely reduced carbon sinks in the Asia-Pacific region but significantly enhanced sinks in India and Africa, with impacts comparable in magnitude to those of the 2015/16 extreme El Niño event. Chen H. et al. (2024) assessed the effects of the 2020-2021 consecutive droughts and large-scale wildfires in southwestern North America. They showed that these events led to a dramatic CO₂ loss from terrestrial ecosystems (95.07 TgC), exceeding 80% of the region's annual carbon sink capacity.

Current limitations in satellite observations, including spatial coverage, revisit frequency, data volume, and measurement accuracy, result in substantial uncertainties in regional terrestrial carbon sink estimates. Inversion results are also influenced by inverse frameworks, a priori emissions and carbon sink fluxes. For example, the common assumption that anthropogenic emissions are fully known introduces unquantifiable errors in estimating both the magnitude and spatial distribution of regional carbon sinks. Furthermore, inconsistencies among satellite XCO₂ datasets remain a critical factor contributing to discrepancies in inversion results. For China's carbon sinks, inversion-based estimates (-0.3 to -1.11 PgC yr⁻¹) vary widely with significant disagreements in spatial distributions (Fig. 4) (Jiang et al., 2016; Wang J. et al., 2020; He W. F. et al., 2022; He et al., 2023b). Zhang L. Y. et al. (2023) used results from 12 ecosystem models as a priori fluxes to estimate terrestrial carbon sinks based on GOSAT XCO2 data. Their study demonstrated that GOSAT observations are only sufficient for reliable estimates at continental scales, while subcontinental or smaller-scale inversions remain heavily dependent on the selection of a priori fluxes due to limited observational constraints. Piao et al. (2022) highlighted in their review that advancing China's next-generation high spatiotemporal resolution GHG monitoring satellites, alongside the establishment of high-resolution radiative transfer models and molecular spectroscopy databases, is imperative to improve the accuracy of XCO₂ observations and enhance the reliability of terrestrial carbon sink inversions in China.

4.3 Methane

Methane (CH₄) is the second-most important anthropogenic GHG, following CO₂. Its global warming potential is 27 times that of CO₂ over a 100-yr horizon and 84 times over a 20-yr horizon (Intergovernmental Panel on Climate Change, 2021). Approximately 60% of global CH₄ emissions originate from human activities, primarily the oil and gas industry, coal mining, livestock farming, rice agriculture, landfills and wastewater treatment. Atmospheric CH₄ concentrations can be monitored via satellite remote sensing with commonly used instruments such as SCIAMACHY (Frankenberg et al., 2005), GOSAT and GOSAT-2 (Parker et al., 2020; Suto et al., 2021), and TROPOMI (Lorente et al., 2021). China's Fengyun and Gaofen satellites are playing increasingly important roles in CH₄ monitoring (Chen L. F. et al., 2021; Yao et al., 2022).

Satellite-based atmospheric CH₄ emission inversions have been used to quantify global CH₄ sources and sinks and to assess CH₄ emission inventories in China (Zhu S. H. et al., 2022; Zhang et al., 2024). For example, Zhang Y. et al. (2021) quantified global CH₄ emissions and sinks from 2010 to 2018 using GOSAT observations. Lu et al. (2022) conducted high-resolution inversion analyses of North American CH₄ emissions by integrating GOSAT satellite data with ground-based and airborne in situ measurements. Zhang et al. (2022), Liang et al. (2023) and Zhao et al. (2024) developed satellite-based high-resolution regional inversion frameworks to estimate the spatial distribution and temporal trends of CH₄ emissions in China. Their findings revealed that China's CH₄ emissions are linked to energy, agricultural, and environmental policies, with an upward trend post 2010 and a decelerated growth rate after 2016.

In-depth studies have been conducted on energy-related CH₄ emissions from oil and gas industries (Zhang Y. Z. et al., 2020; Shen et al., 2022, 2023; Lu et al., 2023; Li F. et al., 2024) and coal mining (Bai et al., 2024; Hu et al., 2024; Tu et al., 2024). Satellite-based inversion estimates indicate that China's total coal mine and oil/gas CH₄ emissions are approximately 20% lower than those derived from bottom-up methods. Specific-

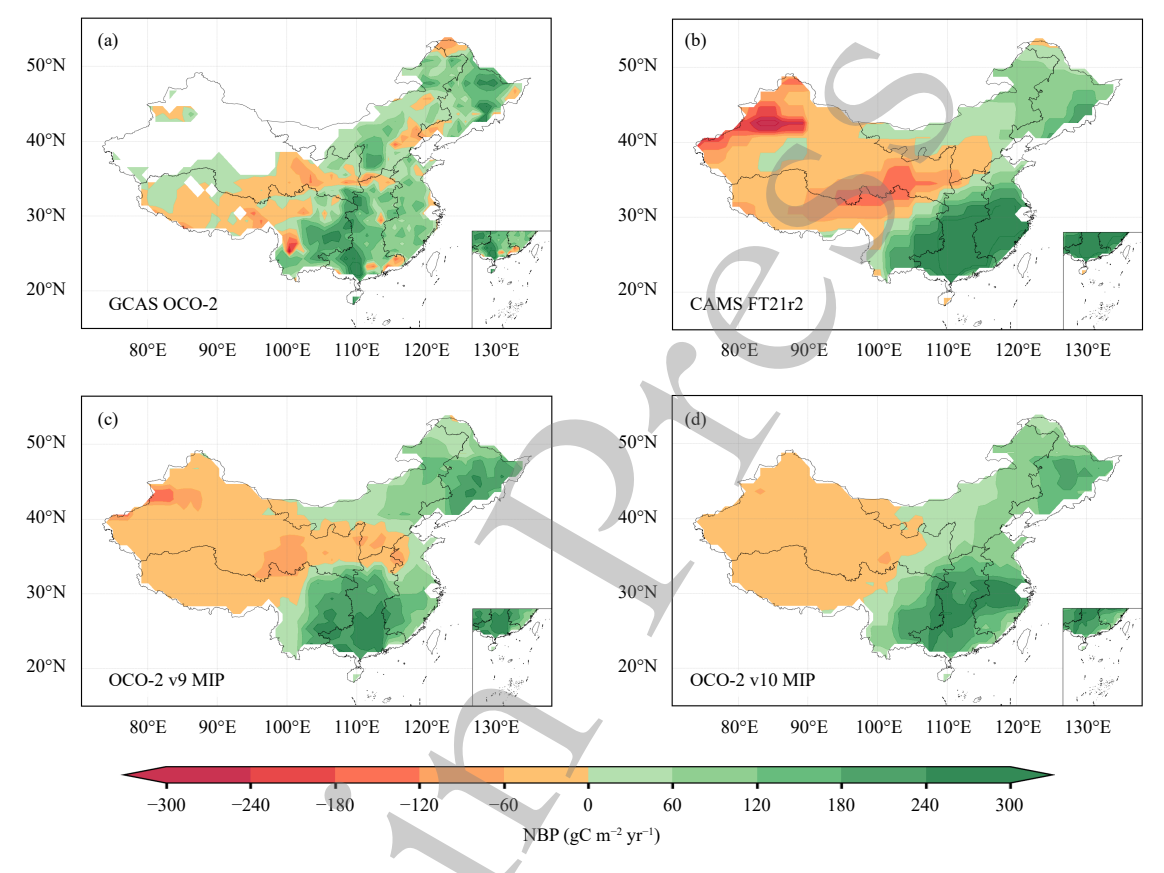


Fig. 4. Annual mean distribution of China's carbon sink, namely, net biome production (NBP, gC m⁻² yr⁻¹) in 2015–2019 constrained with OCO-2 XCO₂ observations, provided by (a) GCAS v2, (b) Copernicus Atmosphere Monitoring Service, and (c, d) NASA OCO-2 Model Intercomparison Project (v9 and v10). Reploted from Fig. 3 in He et al. (2023b).

ally, inversion-derived coal mine emissions are about 12.0-17.5 Tg yr⁻¹, while oil/gas emissions are about 0.72-5.50 Tg yr⁻¹. Satellite observations have significantly reduced estimation biases compared to bottom-up approaches. Be noted that most studies rely on GOSAT data, which suffer from low spatial coverage (with a 260km gap between adjacent observation tracks) and a 3-day revisit cycle, limiting its ability to pinpoint individual anthropogenic emission sources at regional scales. These studies are often conducted at coarse spatial resolutions (200-400 km) (Lu et al., 2021a; Zhang Y. et al., 2021), limiting their ability to differentiate coal mine emissions from other sources. Moreover, the choice of a priori inventory influences inversion results, particularly under sparse satellite data conditions. Recent TROPOMI-based inversions have estimated China's coal mine CH₄ emissions at 15–18 Tg yr⁻¹ with improved spatial resolution (~50 km) (Chen et al., 2022; Liang et al., 2023; Shen et al., 2023), and have detected individual point sources in Shanxi Province (Han et al., 2024). Qin et al. (2023b) proposed integrating multi-source satellite remote sensing and inversion algorithms to develop a coal industry CH₄ emission inventory for China at two distinct scales

including mining clusters and individual mines.

Overall, state-of-the-art satellite remote sensing demonstrates the high timeliness and spatial resolution of CH₄ emission inversions, underscoring their growingly important role in CH₄ mitigation and carbon neutrality. Future GHG monitoring systems should integrate point-source detection/early warning with regional inventory validation to establish a multi-tier observational framework.

5. Summary and biliometric analysis

In summary, substantial progress has been made by Chinese researchers in developing and applying satellitebased emission inversion algorithms for atmospheric pollutants and GHGs.

NO_x emissions have been the most studied target (37.5% of the surveyed papers), with primary inversion methods including local mass balance, Gaussian models, divergence models, and the adjoint of 2D chemical transport models (Fig. 5). The two primary GHGs, CO₂ and CH₄, account for 21.9% and 17.7% of the inversion studies, respectively. For CO₂, the main inversion methods employed are ensemble Kalman filters and Gaussian

models, whereas 3D-Var is predominantly used for CH₄. Despite both being long-lived GHGs, the significant methodological divergence between CO₂ and CH₄ inversions necessitates further research to evaluate its impact on emission assessments. Less attention has been given to pollutants such as NH₃, CO, VOCs, and SO₂. NH₃ studies primarily employ local mass balance and 4D-Var; CO relies on 4D-Var, 3D-Var, and Gaussian models; VOCs utilize diverse methodologies; and SO₂ predominantly applies Gaussian models. Overall, local mass balance, Gaussian models, 3D-Var, ensemble Kalman filter and its variants are the most widely used techniques (Fig. 5). Less prevalent approaches include 4D-Var, divergence models, 2D model adjoint, and machine learning.

The distinct atmospheric lifetimes of GHGs and pollutants significantly influence the selection of inversion methods. For long-lived GHGs, emission inversions must account for long-range transport, making model-simulation-based data assimilation methods the predominant choice. For short-lived air pollutants, regional transport can often be neglected, enabling the use of simplified methods independent of model simulations, but accurately estimating their lifetimes and spatiotemporal variability remains a critical challenge. Specifically, data assimilation methods (4D-Var, 3D-Var, ensemble Kalman filter and its variants) were applied predominantly to GHGs (CO₂ and CH₄) inversions, constituting 73% of the GHG studies. In contrast, simplified methods (local mass balance, Gaussian models, divergence models, and 2D model adjoint) dominate atmospheric pollutant (NO_x, NH₃, VOCs, SO₂, and CO) inversions, accounting for 83% of the studies. It is worth noting that, while the 3D model-based and model-independent methods differ

fundamentally in principle, their applied species show little difference. As shown in Fig. 5, 4D-Var has been leveraged to invert emissions of three pollutants and two GHGs, and Gaussian models have been applied to five pollutants and two GHGs.

The selection of inversion methods and target species is closely linked to advancements in environmental protection policies, computational technologies, and environmental monitoring systems, exhibiting a clear historical evolution trend. As shown in Fig. 6, applications of local mass balance and data assimilation methods have remained stable over time, while the two-dimensional divergence model has seen steady growth since 2022. The use of Gaussian models surged rapidly from 2021, surpassing traditional inversion methods by 2024. Machine learning-based inversions, an emerging approach in 2022, remain in their exploratory phase. From the perspective of target species, NO_r, a dominant atmospheric pollutant, has historically been the most studied. Driven by the urgent need to better understand climate change, the attention to GHGs (CO₂ and CH₄) has risen sharply since 2020. Between 2007 and 2017, one paper was published per year on satellite-based emission inversions on average, whereas annual publication surged to approximately 18 papers during 2022–2024, reflecting explosive growth in this research field.

We emphasize that while this review has endeavored to comprehensively survey Chinese authorship through extensive literature survey, certain omissions may exist due to practical constraints. The limitations could affect the analysis' completeness and accuracy. We apologize for any oversights, and welcome corrections, particularly regarding critical studies not included.

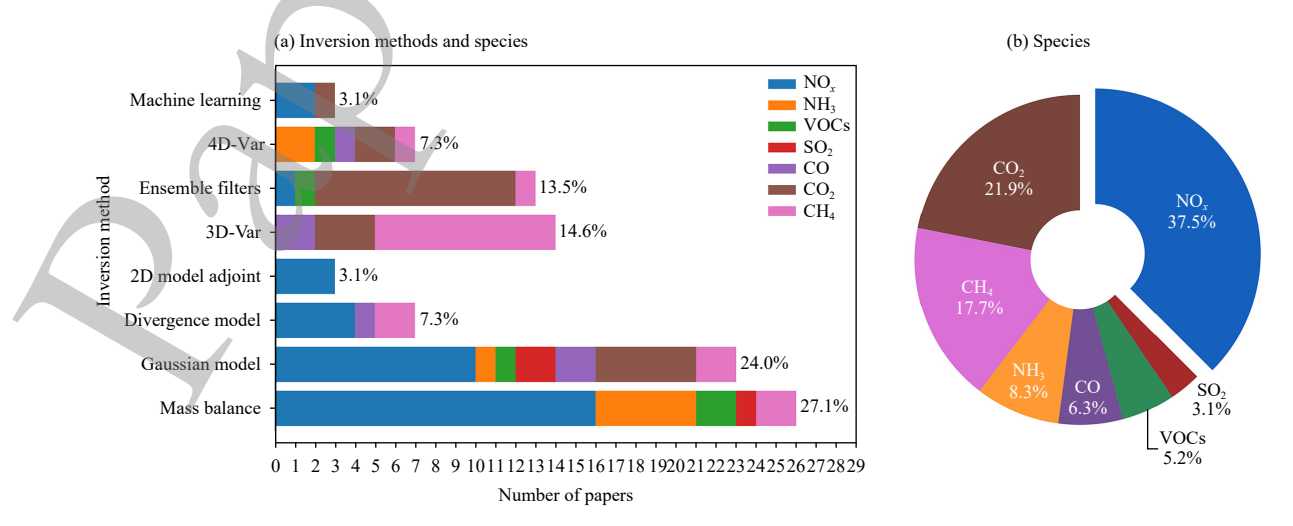


Fig. 5. (a) Inversion methods and (b) target species in the cited papers by Chinese researchers (first affiliation being a Chinese domestic institution). The 3D-Var, 4D-Var, ensemble Kalman filter and its variants are categorized as data assimilation methods; the adjoint of the 2D PHLET model, divergence model, Gaussian model, and local mass balance method are categorized as simplified inversion methods.

6. Discussion and outlook

Satellite-based emission inversions face both challenges and opportunities. The 3D chemical transport models can simulate physical and chemical processes comprehensively, making assimilation methods based on these models theoretically applicable to all types of air pollutants and GHGs. Yet, the high computational resource demand limits the resolution of assimilation results, making it difficult to meet fine-scale environmental management needs. Additionally, data assimilation is sensitive to (systematic) errors in prior emission data,

and is difficult to handle missing emission sources within prior inventories. Data-driven methods such as Gaussian and 2D divergence models do not rely on chemical transport models but are still grounded in physical constraints like mass conservation. These methods do not require prior emission information and can effectively identify missing emission sources in existing emission datasets. The emergence of new-generation high-precision observation platforms like TROPOMI and GEMS has further promoted their application. However, these data-driven methods are difficult to characterize the effects of nonlinear chemical processes, which may lead to

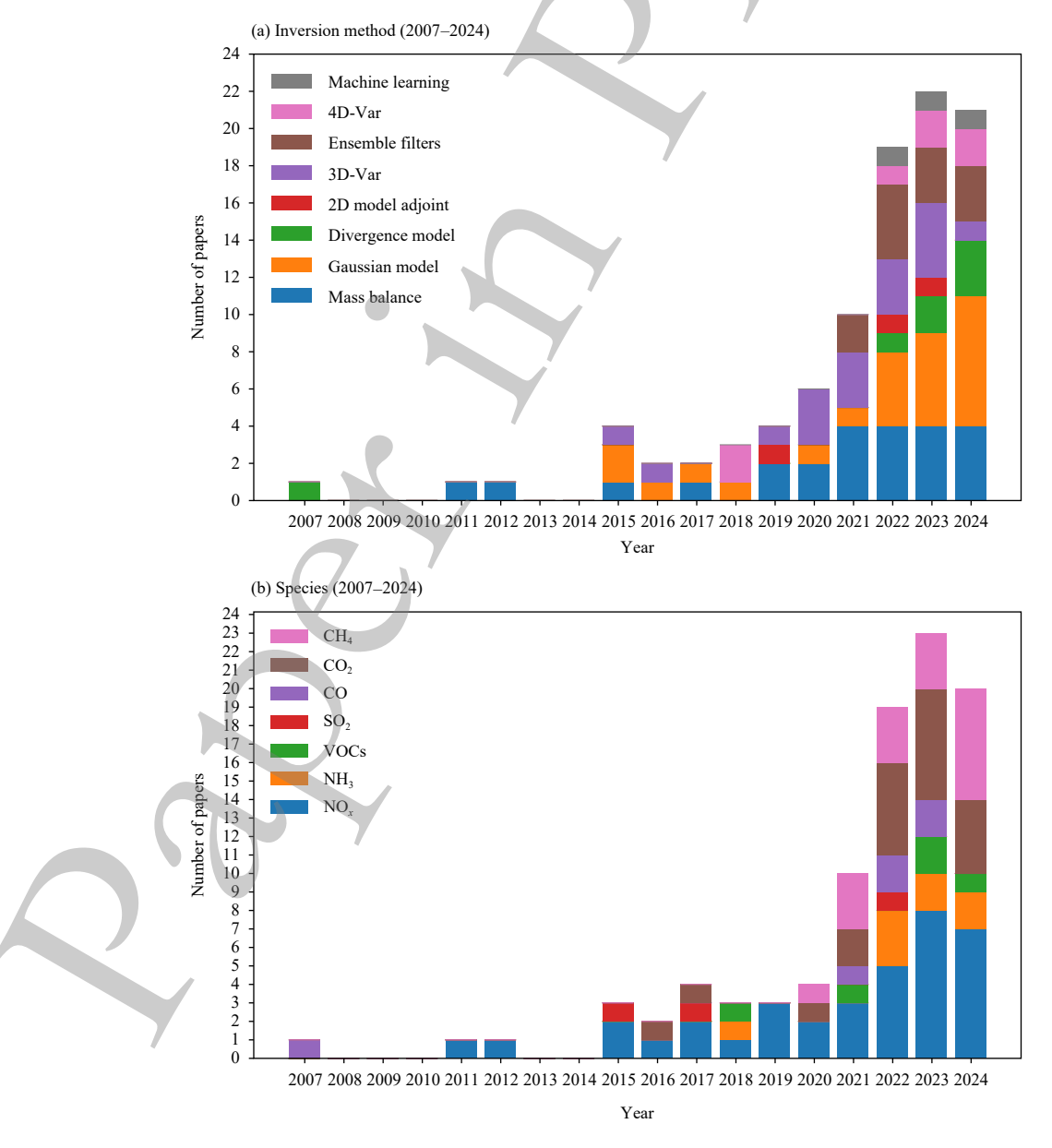


Fig. 6. Historical evolution of (a) inversion methods and (b) target species in the cited papers by Chinese researchers (first affiliation being a Chinese domestic institution). Be noted that the divergence method in Lin et al. (2007) involved chemical transport model, which is different with recent applications of divergence methods that are independent of model simulations.

unreasonable inversion results. For instance, divergence models might produce negative emissions. Through the development of inversion methods, multiple advanced algorithms have been established, some from scratch, to enhance the reliability of inversion results. Given the complementary strengths and weaknesses of model-driven and data-driven inversions, their synergy may open new pathways to diagnose/constrain error sources, thus improving the accuracy of model-driven inversions.

Satellite-based emission inversion results are influenced by both random errors and systematic biases inherent in satellite observations and inversion algorithms. Random errors can be mitigated through expanded observational data or optimized error covariance matrices, vet addressing systematic biases (unknown in general) remains an unresolved critical challenge. Leveraging shared emission sources and chemical linkages among different constituents represents a feasible solution, and attempts have been made in China and elsewhere. From a Bayesian perspective, the addition of independent observational sources can reduce the variance of a posteriori probability distribution. Thus synergy of different types of observational systems becomes paramount—satellites deliver expansive spatial coverage, while ground-based networks supply high-frequency continuous data (Che et al., 2015). Important progress has been made in ground network-based inversions for pollutants and GHGs (Huang et al., 2021; Wu et al., 2023; Zhong et al., 2023; Zhou et al., 2023; Feng et al., 2024). Integrating satellite and ground-based observations to construct a more comprehensive representation of atmospheric processes is expected to reduce the influence of systematic biases.

As an emerging methodology in recent years, machine learning has garnered increasing attention and adoption for emission inversion. It should be noted that machine learning primarily establishes correlation-based mapping functions among input and output variables without explicitly representing physical and chemical processes, potentially leading to inaccurate estimation of pollutant emissions. Future research should prioritize the synergistic integration of physics-based models and machine learning techniques to develop hybrid assimilation algorithms, enabling more robust and comprehensive utilization of observational data. Furthermore, incorporating additional data such as fine-resolution road networks and thermal hotspots, may overcome the inherent limitations of satellite observations, such as resolution, coverage and accuracy, thereby enhancing the spatiotemporal resolution and reliability of inversion-derived emission datasets.

Given the mentioned progress and achievements, non-

etheless, China's emission inversion research efforts are limited by multiple factors such as a relatively late start and a shortage of field experts. Many of the inversion studies have employed the existing theory and methods, with few developed original algorithms. Due to concerns about inversion uncertainties and other factors, the satellite-based emission inversion data have been used mainly as supplements to the conventional "bottom-up" emission inventories or process models; and there is a lack of long-term, multi-constituent, publicly available emission inversion datasets similar to emission inventories. Satellite-based inversion relies on high-quality atmospheric concentration data. In general, China's satellite-based atmospheric environmental remote sensing capabilities still lag behind those in Europe and North America in terms of satellite hardware, spectral data quality, concentration retrieval accuracy, and the level of data openness and sharing. Consequently, current satellite-based inversions in China predominantly rely on foreign satellite spectral/ concentration data, with underdeveloped capabilities for a fully integrated spectrum-concentration-emission inversion system chain using domestic platforms. Furthermore, the absence of satellite observations for N₂O remains a global challenge.

Encouragingly, significant progress has been made in recent years by the Chinese academic community in developing original algorithms, constructing domestic datasets, and enhancing data openness and sharing. China is rapidly advancing its satellite atmospheric monitoring capabilities, with domestically developed platforms such as EMI, GIIRS, TanSat, DQ-1 and OMS now operational. Systematic integration of ground-based, aircraft and mobile observations, coupled with enhanced satelliteground calibration and integrated air-space-ground assessment, would significantly elevate domestic satellite data quality and atmospheric monitoring capability. These efforts would strongly support emission monitoring, inversion, and evaluation. Now, it comes a new opportunity and mission to develop atmospheric pollutant and GHG concentration retrieval products based on domestic satellites and establish a comprehensive emission inversion capability utilizing multi-source domestic and international satellite data, which will provide crutial data and scientific support for environmental governance both in China and globally.

Acknowledgments. The English language in the initial version of this paper was polished by using Chat-GPT and Deepseek, and then undergone multiple rounds of manual revisions.

REFERENCES

- Arellano, A. F., P. S. Kasibhatla, L. Giglio, et al., 2004: Top-down estimates of global CO sources using MOPITT measurements. *Geophys. Res. Lett.*, **31**, L01104, https://doi.org/10.1029/2003GL018609.
- Bai, S. X., Y. G. Zhang, F. Li, et al., 2024: High-resolution satellite estimates of coal mine methane emissions from local to regional scales in Shanxi, China. *Sci. Total Environ.*, **950**, 175446, https://doi.org/10.1016/j.scitotenv.2024.175446.
- Bai, W. G., X. Y. Zhang, and P. Zhang, 2010: Temporal and spatial distribution of tropospheric CO₂ over China based on satellite observations. *Chinese Sci. Bull.*, **55**, 3612–3618, https://doi.org/10.1007/s11434-010-4182-4.
- Beckett, F., E. Rossi, B. Devenish, et al., 2022: Modelling the size distribution of aggregated volcanic ash and implications for operational atmospheric dispersion modelling. *Atmos. Chem. Phys.*, **22**, 3409–3431, https://doi.org/10.5194/acp-22-3409-2022.
- Beer, R., M. W. Shephard, S. S. Kulawik, et al., 2008: First satellite observations of lower tropospheric ammonia and methanol. *Geophys. Res. Lett.*, **35**, L09801, https://doi.org/10.1029/2008GL033642.
- Beirle, S., K. F. Boersma, U. Platt, et al., 2011: Megacity emissions and lifetimes of nitrogen oxides probed from space. *Science*, **333**, 1737–1739, https://doi.org/10.1126/science.12078 24.
- Beirle, S., C. Borger, S. Dörner, et al., 2019: Pinpointing nitrogen oxide emissions from space. *Sci. Adv.*, **5**, eaax9800, https://doi.org/10.1126/sciadv.aax9800.
- Boersma, K. F., H. J. Eskes, J. P. Veefkind, et al., 2007: Near-real time retrieval of tropospheric NO₂ from OMI. *Atmos. Chem. Phys.*, 7, 2103–2118, https://doi.org/10.5194/acp-7-2103-2007.
- Bogumil, K., J. Orphal, T. Homann, et al., 2003: Measurements of molecular absorption spectra with the SCIAMACHY pre-flight model: Instrument characterization and reference data for atmospheric remote-sensing in the 230–2380 nm region. *J. Photochem. Photobiol. A: Chem.*, 157, 167–184, https://doi.org/10.1016/S1010-6030(03)00062-5.
- Burke, M., M. L. Childs, B. De La Cuesta, et al., 2023: The contribution of wildfire to PM_{2.5} trends in the USA. *Nature*, **622**, 761–766, https://doi.org/10.1038/s41586-023-06522-6.
- Butz, A., S. Guerlet, O. Hasekamp, et al., 2011: Toward accurate CO₂ and CH₄ observations from GOSAT. *Geophys. Res. Lett.*, **38**, L14812, https://doi.org/10.1029/2011GL047888.
- Cai, Z. Y., S. Griessbach, and L. Hoffmann, 2022: Improved estimation of volcanic SO₂ injections from satellite retrievals and Lagrangian transport simulations: the 2019 Raikoke eruption. *Atmos. Chem. Phys.*, **22**, 6787–6809, https://doi.org/10.5194/acp-22-6787-2022.
- Cao, H. S., T. M. Fu, L. Zhang, et al., 2018: Adjoint inversion of Chinese non-methane volatile organic compound emissions using space-based observations of formaldehyde and glyoxal. *Atmos. Chem. Phys.*, 18, 15,017–15,046, https://doi.org/10. 5194/acp-18-15017-2018.
- Che, H., X. Y. Zhang, X. Xia, et al., 2015: Ground-based aerosol climatology of China: aerosol optical depths from the China Aerosol Remote Sensing Network (CARSNET) 2002–2013. *Atmos. Chem. Phys.*, **15**, 7619–7652., https://doi.org/10.5194/

- acp-15-7619-2015.
- Chen, H., W. He, J. X. Liu, et al., 2024: Satellite-detected large CO₂ release in southwestern North America during the 2020–2021 drought and associated wildfires. *Environ. Res. Lett.*, **19**, 054047, https://doi.org/10.1088/1748-9326/ad3cf7.
- Chen, L. F., H. Z. Shang, M. Fan, et al., 2021: Mission overview of the GF-5 satellite for atmospheric parameter monitoring. *Natl. Remote Sens. Bull.*, **25**, 1917–1931, https://doi.org/10.11834/jrs.20210582. (in Chinese)
- Chen, P. L., X. X. Xiao, and Q. G. Wang, 2023: High-resolution characteristics of NH₃ emission from 2010 to 2020 in China based on satellite observation. *China Environ. Sci.*, **43**, 2673–2682, https://doi.org/10.3969/j.issn.1000-6923.2023.06.001. (in Chinese)
- Chen, X. K., Z. Jiang, Y. N. Shen, et al., 2024: Ozone mortality burden changes driven by population aging and regional inequity in China in 2013–2050. *GeoHealth*, **8**, e2024GH0 01058, https://doi.org/10.1029/2024GH001058.
- Chen, Y. F., L. Zhang, D. K. Henze, et al., 2021: Interannual variation of reactive nitrogen emissions and their impacts on PM_{2.5} air pollution in China during 2005–2015. *Environ. Res. Let.*, **16**, 125004., https://doi.org/10.1088/1748-9326/ac3695.
- Chen, Z. C., D. J. Jacob, H. Nesser, et al., 2022: Methane emissions from China: A high-resolution inversion of TROPOMI satellite observations. *Atmos. Chem. Phys.*, **22**, 10,809–10,826, https://doi.org/10.5194/acp-22-10809-2022.
- Chen, Z. H., X. Y. Yang, S. Gu, et al., 2019: Spatiotemporal variations and trend analysis of OMI satellite-based tropospheric formaldehyde over China. *Acta Sci. Circumstantiae*, 39, 2852–2859, https://doi.org/10.13671/j.hjkxxb.2019.0209. (in Chinese)
- Clarisse, L., C. Clerbaux, F. Dentener, et al., 2009: Global ammonia distribution derived from infrared satellite observations. *Nat. Geosci.*, **2**, 479–483, https://doi.org/10.1038/ngeo551.
- Crisp, D., H. R. Pollock, R. Rosenberg, et al., 2017: The on-orbit performance of the Orbiting Carbon Observatory-2 (OCO-2) instrument and its radiometrically calibrated products. *Atmos. Meas. Tech.*, 10, 59–81, https://doi.org/10.5194/amt-10-59-2017.
- De Smedt, I., N. Theys, H. Yu, et al., 2018: Algorithm theoretical baseline for formaldehyde retrievals from S5P TROPOMI and from the QA4ECV project. *Atmos. Meas. Tech.*, **11**, 2395–2426, https://doi.org/10.5194/amt-11-2395-2018.
- Deeter, M. N., L. K. Emmons, G. L. Francis, et al., 2003: Operational carbon monoxide retrieval algorithm and selected results for the MOPITT instrument. *J. Geophys. Res. Atmos.*, **108**, 4399, https://doi.org/10.1029/2002JD003186.
- Deng, F., D. B. A. Jones, D. K. Henze, et al., 2014: Inferring regional sources and sinks of atmospheric CO₂ from GOSAT XCO₂ data. *Atmos. Chem. Phys.*, 14, 3703–3727, https://doi.org/10.5194/acp-14-3703-2014.
- Deng, Z., Q. Zhang, X. Zhang, 2021: Satellite-based analysis of spatial-temporal distributions of NH₃ and factors of influence in North China. *Front. Environ. Sci.*, 9, 761557, https:// doi.org/10.3389/fenvs.2021.761557.
- Duncan, B. N., L. N. Lamsal, A. M. Thompson, et al., 2016: A space-based, high-resolution view of notable changes in urb-an NO_x pollution around the world (2005–2014). *J. Geophys. Res. Atmos.*, **121**, 976–996, https://doi.org/10.1002/2015JD02

4121.

- Elbern, H., H. Schmidt, O. Talagrand, et al., 2000: 4D-variational data assimilation with an adjoint air quality model for emission analysis. *Environ. Model. Softw.*, **15**, 539–548, https://doi.org/10.1016/S1364-8152(00)00049-9.
- Eldering, A., T. E. Taylor, C. W. O'dell, et al., 2019: The OCO-3 mission: measurement objectives and expected performance based on 1 year of simulated data. *Atmos. Meas. Tech.*, **12**, 2341–2370, https://doi.org/10.5194/amt-12-2341-2019.
- Feng, S. Z., F. Jiang, H. M. Wang, et al., 2024: China's fossil fuel CO₂ emissions estimated using surface observations of coemitted NO₂. *Environ. Sci. Technol.*, **58**, 8299–8312, https://doi.org/10.1021/acs.est.3c07756.
- Frankenberg, C., U. Platt, and T. Wagner, 2005: Iterative maximum a posteriori (IMAP)-DOAS for retrieval of strongly absorbing trace gases: Model studies for CH₄ and CO₂ retrieval from near infrared spectra of SCIAMACHY onboard ENVISAT. *Atmos. Chem. Phys.*, **5**, 9–22, https://doi.org/10.5194/acp-5-9-2005.
- Friedlingstein, P., M. O'sullivan, M. W. Jones, et al., 2023: Global carbon budget 2023. *Earth Syst. Sci. Data*, **15**, 5301–5369, https://doi.org/10.5194/essd-15-5301-2023.
- Fu, T. M., D. J. Jacob, P. I. Palmer, et al., 2007: Space-based form-aldehyde measurements as constraints on volatile organic compound emissions in east and south Asia and implications for ozone. *J. Geophys. Res. Atmos.*, **112**, D06312, https://doi.org/10.1029/2006JD007853.
- Ge, X. R., M. Schaap, R. Kranenburg, et al., 2020: Modeling atmospheric ammonia using agricultural emissions with improved spatial variability and temporal dynamics. *Atmos. Chem. Phys.*, 20, 16,055–16,087, https://doi.org/10.5194/acp-20-16055-2020.
- George, M., C. Clerbaux, D. Hurtmans, et al., 2009: Carbon monoxide distributions from the IASI/METOP mission: Evaluation with other space-borne remote sensors. *Atmos. Chem. Phys.*, **9**, 8317–8330, https://doi.org/10.5194/acp-9-8317-2009.
- González Abad, G., X. Liu, K. Chance, et al., 2015: Updated Smithsonian Astrophysical Observatory Ozone Monitoring Instrument (SAO OMI) formaldehyde retrieval. *Atmos. Meas. Tech.*, **8**, 19–32, https://doi.org/10.5194/amt-8-19-2015.
- Goodfellow, I., I. Bengio, and A. Courville, 2016: *Deep Learning*. MIT Press, pp. 800.
- Gu, D. S., Y. H. Wang, C. Smeltzer, et al., 2014: Anthropogenic emissions of NO_x over China: Reconciling the difference of inverse modeling results using GOME-2 and OMI measurements. *J. Geophys. Res. Atmos.*, 119, 7732–7740, https://doi. org/10.1002/2014JD021644.
- Gu, D. S., Y. H. Wang, R. Yin, et al., 2016: Inverse modelling of NO_x emissions over eastern China: Uncertainties due to chemical non-linearity. *Atmos. Meas. Tech.*, **9**, 5193–5201, https://doi.org/10.5194/amt-9-5193-2016.
- Guo, W. Y., Y. S. Shi, Y. Liu, et al., 2023: CO₂ emissions retrieval from coal-fired power plants based on OCO-2/3 satellite observations and a Gaussian plume model. *J. Clean. Prod.*, **397**, 136525, https://doi.org/10.1016/j.jclepro.2023.136525.
- Han, G., H. Xu, W. Gong, et al., 2018: Feasibility study on measuring atmospheric CO₂ in urban areas using spaceborne CO₂-IPDA LIDAR. *Remote Sens.*, **10**, 985, https://doi.org/10.3390/rs10070985.

- Han, G., Z. P. Pei, T. Q. Shi, et al., 2024: Unveiling unprecedented methane hotspots in China's leading coal production hub: A satellite mapping revelation. *Geophys. Res. Lett.*, 51, e2024GL109065, https://doi.org/10.1029/2024GL109065.
- Han, X., J. Yang, S. Tang, et al., 2020: Vegetation products derived from Fengyun-3D medium resolution spectral imager-II. J. Meteor. Res., 34, 775–785, https://doi.org/10.1007/s13351-020-0027-5.
- He, C., X. Lu, Y. Z. Zhang, et al., 2024: Revisiting the quantification of power plant CO₂ emissions in the United States and China from satellite: A comparative study using three top-down approaches. *Remote Sens. Environ.*, 308, 114192, https://doi.org/10.1016/j.rse.2024.114192.
- He, J. H., Y. L. Cai, and P. Qin, 2020: Spatial and temporal variations of carbon dioxide and its influencing factors. *Chinese Sci. Bull.*, **65**, 194–202, https://doi.org/10.1360/TB-2019-0022. (in Chinese)
- He, T. L., D. B. A. Jones, K. Miyazaki, et al., 2022: Inverse modelling of Chinese NO_x emissions using deep learning: Integrating in situ observations with a satellite-based chemical reanalysis. *Atmos. Chem. Phys.*, **22**, 14,059–14,074, https://doi.org/10.5194/acp-22-14059-2022.
- He, W. F. Jiang, M. S. Wu, et al., 2022: China's terrestrial carbon sink over 2010–2015 constrained by satellite observations of atmospheric CO₂ and land surface variables. *J. Geophys. Res. Biogeo.*, **127**, e2021JG006644, https://doi.org/10.1029/2021JG006644.
- He, W., F. Jiang, W. M. Ju, et al., 2023a: Do state-of-the-art atmospheric CO₂ inverse models capture drought impacts on the european land carbon uptake. *J. Adv. Model. Earth Syst.*, **15**, e2022MS003150, https://doi.org/10.1029/2022MS003150.
- He, W., F. Jiang, W. M. Ju, et al., 2023b: Improved constraints on the recent terrestrial carbon sink over China by assimilating OCO-2 XCO₂ retrievals. *J. Geophys. Res. Atmos.*, **128**, e2022JD037773, https://doi.org/10.1029/2022JD037773.
- Hedelius, J. K., G. C. Toon, R. R. Buchholz, et al., 2021: Regional and urban column CO trends and anomalies as observed by MOPITT over 16 years. *J. Geophys. Res. Atmos.*, **126**, e2020JD033967, https://doi.org/10.1029/2020JD033967.
- Henze, D. K., A. Hakami, and J. H. Seinfeld, 2007: Development of the adjoint of GEOS-Chem. *Atmos. Chem. Phys.*, 7, 2413–2433, https://doi.org/10.5194/acp-7-2413-2007.
- Hoegh-Guldberg, O., D. Jacob, M. Taylor, et al., 2019: The human imperative of stabilizing global climate change at 1.5°C. *Science*, **365**, eaaw6974, https://doi.org/10.1126/science.aaw6974.
- Hong, X., P. Zhang, Y. Bi, et al., 2022: Retrieval of Global Carbon Dioxide From TanSat Satellite and Comprehensive Validation With TCCON Measurements and Satellite Observations. *IEEE Trans. Geosci. Remote Sens.*, 60, 4101716., https://doi.org/10.1109/tgrs.2021.3066623.
- Hsu, C. H., D. K. Henze, A. P. Mizzi, et al., 2024: An observing system simulation experiment analysis of how well geostationary satellite trace-gas observations constrain NO_x emissions in the US. *J. Geophys. Res. Atmos.*, **129**, e2023JD0 39323, https://doi.org/10.1029/2023JD039323.
- Hu, W., K. Qin, F. Lu, et al., 2024: Merging TROPOMI and eddy covariance observations to quantify 5-years of daily CH₄ emissions over coal-mine dominated region. *Int. J. Coal Sci.*

- Technol., 11, 56, https://doi.org/10.1007/s40789-024-00700-1.
- Hu, Y. Q., and Y. S. Shi, 2021: Estimating CO₂ emissions from large scale coal-fired power plants using OCO-2 observations and emission inventories. *Atmosphere*, 12, 811, https://doi. org/10.3390/atmos12070811.
- Hu, Y. W., Z. L. Zang, X. Y. Ma, et al., 2022: Four-dimensional variational assimilation for SO₂ emission and its application around the COVID-19 lockdown in the spring 2020 over China. *Atmos. Chem. Phys.*, 22, 13183–13200, https://doi.org/10.5194/acp-22-13183-2022.
- Huang, L., S. Liu, Z. Y. Yang, et al., 2021: Exploring deep learning for air pollutant emission estimation. *Geosci. Model Dev.*, **14**, 4641–4654, https://doi.org/10.5194/gmd-14-4641-2021.
- Huang, X. Y., V. Srikrishnan, J. Lamontagne, et al., 2023: Effects of global climate mitigation on regional air quality and health. *Nat. Sustain.*, 6, 1054–1066, https://doi.org/10.1038/s41893-023-01133-5.
- Hunt, B. R., E. J. Kostelich, and I. Szunyogh, 2007: Efficient data assimilation for spatiotemporal chaos: A local ensemble transform Kalman filter. *Phys. D: Nonlinear Phenom.*, 230, 112–126, https://doi.org/10.1016/j.physd.2006.11.008.
- Intergovernmental Panel on Climate Change, 2023: Short-lived climate forcers. *Climate Change 2021: The Physical Science Basis*, V. Masson-Delmotte, P. Zhai, A. Pirani, et al., Ed., Cambridge University Press, Cambridge, United Kingdom, 817–922, doi: 10.1017/9781009157896.008.
- Jiang, F., J. M. Chen, L. X. Zhou, et al., 2016: A comprehensive estimate of recent carbon sinks in China using both top-down and bottom-up approaches. *Sci. Rep.*, **6**, 22130, https://doi.org/10.1038/srep22130.
- Jiang, F., W. M. Ju, W. He, et al., 2022: A 10-year global monthly averaged terrestrial net ecosystem exchange dataset inferred from the ACOS GOSAT v9 XCO₂ retrievals (GCAS2021). *Earth Syst. Sci. Data*, 14, 3013–3037, https://doi.org/10.5194/ essd-14-3013-2022.
- Jiang, Z., D. B. A. Jones, M. Kopacz, et al., 2011: Quantifying the impact of model errors on top-down estimates of carbon monoxide emissions using satellite observations. *J. Geophys. Res. Atmos.*, 116, D15306, https://doi.org/10.1029/2010JD0 15282.
- Jiang, Z., D. B. A. Jones, J. Worden, et al., 2015: Regional data assimilation of multi-spectral MOPITT observations of CO over North America. *Atmos. Chem. Phys.*, 15, 6801–6814, https://doi.org/10.5194/acp-15-6801-2015.
- Jiang, Z., J. R. Worden, H. Worden, et al., 2017: A 15-year record of CO emissions constrained by MOPITT CO observations. *Atmos. Chem. Phys.*, 17, 4565–4583, https://doi.org/10.5194/acp-17-4565-2017.
- Jiang, Z., B. C. Mcdonald, H. Worden, et al., 2018: Unexpected slowdown of US pollutant emission reduction in the past decade. *Proc. Natl. Acad. Sci. USA*, 115, 5099–5104, https://doi. org/10.1073/pnas.1801191115.
- Jiang, Z., R. Zhu, K. Miyazaki, et al., 2022: Decadal variabilities in tropospheric nitrogen oxides over United States, Europe, and China. *J. Geophys. Res. Atmos.*, 127, e2021JD0358 72, https://doi.org/10.1029/2021JD035872.
- Jin, J. B., L. Fang, B. J. Li, et al., 2023: 4DEnVar-based inversion system for ammonia emission estimation in China through assimilating IASI ammonia retrievals. *Environ. Res. Lett.*, 18,

- 034005, https://doi.org/10.1088/1748-9326/acb835.
- Jin, Z., X. J. Tian, Y. L. Wang, et al., 2024: A global surface CO₂ flux dataset (2015–2022) inferred from OCO-2 retrievals using the GONGGA inversion system. *Earth Syst. Sci. Data*, 16, 2857–2876, https://doi.org/10.5194/essd-16-2857-2024.
- Jones, D. B. A., K. W. Bowman, J. A. Logan, et al., 2009: The zonal structure of tropical O₃ and CO as observed by the Tropospheric Emission Spectrometer in November 2004 – Part 1: Inverse modeling of CO emissions. *Atmos. Chem. Phys.*, 9, 3547–3562, https://doi.org/10.5194/acp-9-3547-2009.
- Kim, J., U. Jeong, M. H. Ahn, et al., 2020: New era of air quality monitoring from space: Geostationary Environment Monitoring Spectrometer (GEMS). *Bull. Amer. Meteor. Soc.*, 101, E1–E22, https://doi.org/10.1175/BAMS-D-18-0013.1.
- Kong, H., J. T. Lin, R. X. Zhang, et al., 2019: High-resolution (0.05° × 0.05°) NO_x emissions in the Yangtze River Delta inferred from OMI. *Atmos. Chem. Phys.*, **19**, 12835–12856, https://doi.org/10.5194/acp-19-12835-2019.
- Kong, H., J. T. Lin, L. L. Chen, et al., 2022: Considerable unaccounted local sources of NO_x emissions in China revealed from satellite. *Environ. Sci. Technol.*, **56**, 7131–7142, https://doi.org/10.1021/acs.est.1c07723.
- Kong, H., J. T. Lin, Y. H. Zhang, et al., 2023: High natural nitric oxide emissions from lakes on Tibetan Plateau under rapid warming. *Nat. Geosci.*, **16**, 474–477, https://doi.org/10.1038/s41561-023-01200-8.
- Kong, Y. W., B. Zheng, Q. Zhang, et al., 2022: Global and regional carbon budget for 2015–2020 inferred from OCO-2 based on an ensemble Kalman filter coupled with GEOS-Chem. *Atmos. Chem. Phys.*, 22, 10769–10788, https://doi.org/10.5194/acp-22-10769-2022.
- Kou, X. X., Z. Peng, M. G. Zhang, et al., 2023: The carbon sink in China as seen from GOSAT with a regional inversion system based on the Community Multi-scale Air Quality (CMAQ) and ensemble Kalman smoother (EnKS). *Atmos. Chem. Phys.*, 23, 6719–6741, https://doi.org/10.5194/acp-23-6719-2023.
- Kwon, H. A., R. J. Park, G. González Abad, et al., 2019: Description of a formaldehyde retrieval algorithm for the Geostationary Environment Monitoring Spectrometer (GEMS). *Atmos. Meas. Tech.*, 12, 3551–3571, https://doi.org/10.5194/amt-12-3551-2019.
- Lamsal, L. N., R. V. Martin, A. Padmanabhan, et al., 2011: Application of satellite observations for timely updates to global anthropogenic NO_x emission inventories. *Geophys. Res. Lett.*, **38**, L05810, https://doi.org/10.1029/2010GL046476.
- Landgraf, J., J. Aan De brugh, R. Scheepmaker, et al., 2016: Carbon monoxide total column retrievals from TROPOMI shortwave infrared measurements. *Atmos. Meas. Tech.*, **9**, 4955–4975, https://doi.org/10.5194/amt-9-4955-2016.
- Le Quéré, C., R. J. Andres, T. Boden, et al., 2013: The global carbon budget 1959–2011. *Earth Syst. Sci. Data*, **5**, 165–185, https://doi.org/10.5194/essd-5-165-2013.
- LeCun, Y., Y. Bengio, and G. Hinton, 2015: Deep learning. *Nature*, **521**, 436–444, https://doi.org/10.1038/nature14539.
- Li, B. J., L. Chen, W. S. Shen, et al., 2021: Improved gridded ammonia emission inventory in China. *Atmos. Chem. Phys.*, 21, 15883–15900, https://doi.org/10.5194/acp-21-15883-2021.
- Li, C., N. A. Krotkov, J. Joiner, et al., 2024: Version 1 NOAA-20/OMPS nadir mapper total column SO₂ product: Continu-

- ation of NASA long-term global data record. *Earth Syst. Sci. Data*, **16**, 4291–4309, https://doi.org/10.5194/essd-16-4291-2024
- Li, F., S. X. Bai, K. E. Lin, et al., 2024: Satellite-based surveys reveal substantial methane point-source emissions in major oil & gas basins of North America During 2022–2023. *J. Geophys. Res. Atmos.*, 129, e2024JD040870, https://doi.org/10.1029/2024JD040870.
- Li, H., B. Zheng, P. Ciais, et al., 2023: Satellite reveals a steep decline in China's CO₂ emissions in early 2022. *Sci. Adv.*, 9, eadg7429, https://doi.org/10.1126/sciadv.adg7429.
- Li, H., B. Zheng, Y. Lei, et al., 2024: Trends and drivers of anthropogenic NO_x emissions in China since 2020. *Environ. Sci. Ecotechnol.*, **21**, 100425, https://doi.org/10.1016/j.ese.2024. 100425.
- Li, J., X. Zhang, L. Guo, et al., 2024: Invert global and China's terrestrial carbon fluxes over 2019–2021 based on assimilating richer atmospheric CO₂ observations. *Sci. Total Environ.*, 929, 172320, https://doi.org/10.1016/j.scitotenv.2024.172320.
- Li, L., H. Che, Y. Derimian, et al., 2020: Climatology of fine and coarse mode aerosol optical thickness over East and South Asia derived from POLDER/PARASOL satellite. *J. Geophys. Res. Atmos.*, **125**, e2020JD032665, https://doi.org/10.1029/2020jd032665.
- Li, M., Z. Klimont, Q. Zhang, et al., 2018: Comparison and evaluation of anthropogenic emissions of SO₂ and NO_x over China. *Atmos. Chem. Phys.*, **18**, 3433–3456, https://doi.org/10.5194/acp-18-3433-2018.
- Li, S. W., and J. Xing, 2024: DeepSAT4D: Deep learning empowers four-dimensional atmospheric chemical concentration and emission retrieval from satellite. *Innov. Geosci.*, 2, 100061, https://doi.org/10.59717/j.xinn-geo.2024.100061.
- Li, W., X. Han, J. L. Li, et al., 2023: Assessment of surface ozone production in Qinghai, China with satellite-constrained VOCs and NO_x emissions. *Sci. Total Environ.*, **905**, 166602, https://doi.org/10.1016/j.scitotenv.2023.166602.
- Li, X. L., J. B. Cohen, K. Qin, et al., 2023: Remotely sensed and surface measurement-derived mass-conserving inversion of daily NO_x emissions and inferred combustion technologies in energy-rich northern China. *Atmos. Chem. Phys.*, **23**, 8001–8019, https://doi.org/10.5194/acp-23-8001-2023.
- Li, Y. S., Y. X. Zheng, M. Y. Liu, et al., 2018: Satellite-based observations of changes in nitrogen oxides over the Beijing—Tianjin–Hebei region from 2011 to 2017. *Acta Sci. Circumstantiae*, **38**, 3797–3806, https://doi.org/10.13671/j.hjkxxb. 2018.0219.
- Liang, R. S., Y. Z. Zhang, W. Chen, et al., 2023: East Asian methane emissions inferred from high-resolution inversions of GOSAT and TROPOMI observations: A comparative and evaluative analysis. *Atmos. Chem. Phys.*, **23**, 8039–8057, https://doi.org/10.5194/acp-23-8039-2023.
- Lin, J. T., 2012: Satellite constraint for emissions of nitrogen oxides from anthropogenic, lightning and soil sources over East China on a high-resolution grid. *Atmos. Chem. Phys.*, **12**, 2881–2898, https://doi.org/10.5194/acp-12-2881-2012.
- Lin, J. T., and M. B. McElroy, 2011: Detection from space of a reduction in anthropogenic emissions of nitrogen oxides during the Chinese economic downturn. *Atmos. Chem. Phys.*, **11**, 8171–8188, https://doi.org/10.5194/acp-11-8171-2011.

- Lin, J. T., M. B. Mcelroy, and K. F. Boersma, 2010: Constraint of anthropogenic NO_x emissions in China from different sectors:
 A new methodology using multiple satellite retrievals. *Atmos. Chem. Phys.*, 10, 63–78, https://doi.org/10.5194/acp-10-63-2010
- Lin, J. T., M. Y. Liu, J. Y. Xin, et al., 2015: Influence of aerosols and surface reflectance on satellite NO₂ retrieval: Seasonal and spatial characteristics and implications for NO_x emission constraints. *Atmos. Chem. Phys.*, **15**, 11217–11241, https://doi.org/10.5194/acp-15-11217-2015.
- Lin, X. J., A. R. Van Der, J. De Laat, et al., 2023: Monitoring and quantifying CO₂ emissions of isolated power plants from space. *Atmos. Chem. Phys.*, **23**, 6599–6611, https://doi.org/10.5194/acp-23-6599-2023.
- Lin, Y. P., C. S. Zhao, L. Peng, et al., 2007: A new method to calculate monthly CO emissions using MOPITT satellite data. *Chinese Sci. Bull.*, **52**, 2551–2558, https://doi.org/10.1007/s11434-007-0349-z.
- Liu, C., W. G. Liu, P. Zhang, et al., 2013: The inverse method of carbon monoxide from satellite measurement and the result analysis. *Acta. Phys. Sinica*, **62**, 030704, https://doi.org/10.7498/aps.62.030704. (in Chinese)
- Liu, F., S. Beirle, Q. Zhang, et al., 2016: NO_x lifetimes and emissions of cities and power plants in polluted background estimated by satellite observations. *Atmos. Chem. Phys.*, **16**, 5283–5298, https://doi.org/10.5194/acp-16-5283-2016.
- Liu, F., S. Beirle, Q. Zhang, et al., 2017: NO_x emission trends over Chinese cities estimated from OMI observations during 2005 to 2015. *Atmos. Chem. Phys.*, **17**, 9261–9275, https://doi.org/10.5194/acp-17-9261-2017.
- Liu, J., J. B. Cohen, Q. He, et al., 2024: Accounting for NO_x emissions from biomass burning and urbanization doubles existing inventories over South, Southeast and East Asia. *Commun. Earth Environ.*, 5, 255, https://doi.org/10.1038/s43247-024-01424-5.
- Liu, J. J., K. W. Bowman, D. S. Schimel, et al., 2017: Contrasting carbon cycle responses of the tropical continents to the 2015–2016 El Niño. *Science*, **358**, eaam5690, https://doi.org/10.1126/science.aam5690.
- Liu, P., J. Ding, L. Liu, et al., 2022a: Estimation of surface ammonia concentrations and emissions in China from the polar-orbiting Infrared Atmospheric Sounding Interferometer and the FY-4A Geostationary Interferometric Infrared Sounder. *Atmos. Chem. Phys.*, 22, 9099–9110, https://doi.org/10.5194/acp-22-9099-2022.
- Liu, P., J. Ding, Y. F. Ji, et al., 2022b: Satellite support to estimate livestock ammonia emissions: A case study in Hebei, China. *Atmosphere*, 13, 1552, https://doi.org/10.3390/atmos13101552
- Liu, S., X. C. Li, J. Li, et al., 2023: Observing network effect of shipping emissions from space: A natural experiment in the world's busiest port. *PNAS Nexus*, 2, pgad391, https://doi.org/ 10.1093/pnasnexus/pgad391.
- Liu, Y., J. Wang, L. Yao, et al., 2018: The TanSat mission: Preliminary global observations. Sci. Bull., 63, 1200–1207, https://doi.org/10.1016/j.scib.2018.08.004.
- Lorente, A., T. Borsdorff, A. Butz, et al., 2021: Methane retrieved from TROPOMI: Improvement of the data product and validation of the first 2 years of measurements. *Atmos. Meas.*

- Tech., 14, 665–684, https://doi.org/10.5194/amt-14-665-2021.
- Lu, X., D. J. Jacob, Y. Z. Zhang, et al., 2021a: Global methane budget and trend, 2010–2017: Complementarity of inverse analyses using in situ (GLOBALVIEW plus CH₄ ObsPack) and satellite (GOSAT) observations. *Atmos. Chem. Phys.*, 21, 4637–4657, https://doi.org/10.5194/acp-21-4637-2021.
- Lu, X., X. P. Ye, M. Zhou, et al., 2021b: The underappreciated role of agricultural soil nitrogen oxide emissions in ozone pollution regulation in North China. *Nat. Commun.*, **12**, 5021, https://doi.org/10.1038/s41467-021-25147-9.
- Lu, X., D. J. Jacob, H. L. Wang, et al., 2022: Methane emissions in the United States, Canada, and Mexico: Evaluation of national methane emission inventories and 2010–2017 sectoral trends by inverse analysis of in situ (GLOBALVIEWplus CH₄ ObsPack) and satellite (GOSAT) atmospheric observations. *Atmos. Chem. Phys.*, 22, 395–418, https://doi.org/10. 5194/acp-22-395-2022.
- Lu, X., D. J. Jacob, Y. Z. Zhang, et al., 2023: Observation-derived 2010–2019 trends in methane emissions and intensities from US oil and gas fields tied to activity metrics. *Proc. Natl. Acad. Sci. USA*, 120, e2217900120, https://doi.org/10.1073/pnas.2217900120.
- Luo, Z. Q., Y. Z. Zhang, W. Chen, et al., 2022: Estimating global ammonia (NH₃) emissions based on IASI observations from 2008 to 2018. *Atmos. Chem. Phys.*, **22**, 10,375–10,388, https://doi.org/10.5194/acp-22-10375-2022.
- Luo, Z. Y., T. K. He, W. Yi, et al., 2023: Advancing shipping NO_x pollution estimation through a satellite-based approach. *PNAS Nexus*, **3**, pgad430, https://doi.org/10.1093/pnasnexus/pgad430.
- Martin, R. V., K. Chance, D. J. Jacob, et al., 2002: An improved retrieval of tropospheric nitrogen dioxide from GOME. *J. Geophys. Res. Atmos.*, **107**, 4437, https://doi.org/10.1029/2001JD001027.
- Martin, R. V., D. J. Jacob, K. Chance, et al., 2003: Global inventory of nitrogen oxide emissions constrained by space-based observations of NO₂ columns. *J. Geophys. Res. Atmos.*, **108**, 4537, https://doi.org/10.1029/2003JD003453.
- McMillan, W. W., C. Barnet, L. Strow, et al., 2005: Daily global maps of carbon monoxide from NASA's Atmospheric Infrared Sounder. *Geophys. Res. Lett.*, 32, L11801, https://doi. org/10.1029/2004GL021821.
- Miyazaki, K., H. J. Eskes, K. Sudo, et al., 2012: Simultaneous assimilation of satellite NO₂, O₃, CO, and HNO₃ data for the analysis of tropospheric chemical composition and emissions. *Atmos. Chem. Phys.*, **12**, 9545–9579, https://doi.org/10.5194/acp-12-9545-2012.
- Miyazaki, K., K. Bowman, T. Sekiya, et al., 2020: Updated tropospheric chemistry reanalysis and emission estimates, TCR-2, for 2005–2018. *Earth Syst. Sci. Data*, **12**, 2223–2259, https://doi.org/10.5194/essd-12-2223-2020.
- Nassar, R., T. G. Hill, C. A. Mclinden, et al., 2017: Quantifying CO₂ emissions from individual power plants from space. *Geophys. Res. Lett.*, 44, 10045–10053, https://doi.org/10.1002/2017GL074702.
- Nassar, R., J. P. Mastrogiacomo, W. Bateman-Hemphill, et al., 2021: Advances in quantifying power plant CO₂ emissions with OCO-2. *Remote Sens. Environ.*, **264**, 112579, https://doi.org/10.1016/j.rse.2021.112579.

- Nowlan, C. R., G. González Abad, H. A. Kwon, et al., 2023: Global formaldehyde products from the Ozone Mapping and Profiler Suite (OMPS) nadir mappers on suomi NPP and NOAA-20. *Earth Space Sci.*, 10, e2022EA002643, https://doi.org/10.1029/2022EA002643.
- Pan, Y. Q., L. Duan, M. Q. Li, et al., 2023: Widespread missing super-emitters of nitrogen oxides across China inferred from year-round satellite observations. *Sci. Total Environ.*, 864, 161157, https://doi.org/10.1016/j.scitotenv.2022.161157.
- Parker, R. J., A. Webb, H. Boesch, et al., 2020: A decade of GOS-AT Proxy satellite CH₄ observations. *Earth Syst. Sci. Data*, 12, 3383–3412, https://doi.org/10.5194/essd-12-3383-2020.
- Pérez-Invernón, F. J., F. J. Gordillo-vázquez, O. Van Der velde, et al., 2023: Lightning-produced nitrogen oxides per flash length obtained by using TROPOMI observations and the ebro lightning mapping array. *Geophys. Res. Lett.*, 50, e2023GL 104699, https://doi.org/10.1029/2023GL104699.
- Piao, S., Y. He, X. H. Wang, et al., 2022: Estimation of China's terrestrial ecosystem carbon sink: Methods, progress and prospects. *Sci. China Earth Sci.*, **65**, 641–651, https://doi.org/10.1007/s11430-021-9892-6.
- Pu, D. C., L. Zhu, H. Z. Shen, et al., 2024: Integrated satellite observations unravel the relationship between urbanization and anthropogenic non-methane volatile organic compound emissions globally. *npj Climate Atmos. Sci*, 7, 125, https://doi.org/10.1038/s41612-024-00683-5.
- Qin, K., L. X. Lu, J. Liu, et al., 2023a: Model-free daily inversion of NO_x emissions using TROPOMI (MCMFE-NO_x) and its uncertainty: Declining regulated emissions and growth of new sources. *Remote Sens. Environ.*, **295**, 113720, https://doi.org/10.1016/j.rse.2023.113720.
- Qin, K., Q. He, H. S. Kang, et al., 2023b: Progress and prospect of satellite remote sensing research applied to methane emissions from the coal industry. *Acta Opt. Sinica*, **43**, 1899908, https://doi.org/10.3788/AOS231293. (in Chinese)
- Qu, Z., D. K. Henze, H. M. Worden, et al., 2022: Sector-based top-down estimates of NO_x, SO₂, and CO emissions in East Asia. *Geophys. Res. Lett.*, 49, e2021GL096009, https://doi.org/10.1029/2021GL096009.
- Ren, J., F. F. Guo, and S. D. Xie, 2022: Diagnosing ozone–NO_x–VOC sensitivity and revealing causes of ozone increases in China based on 2013–2021 satellite retrievals. *Atmos. Chem. Phys.*, **22**, 15035–15047, https://doi.org/10.5194/acp-22-15035-2022.
- Reuter, M., M. Buchwitz, O. Schneising, et al., 2019: Towards monitoring localized CO₂ emissions from space: Co-located regional CO₂ and NO₂ enhancements observed by the OCO-2 and S5P satellites. *Atmos. Chem. Phys.*, **19**, 9371–9383, https://doi.org/10.5194/acp-19-9371-2019.
- Rodgers, C. D., 2000: Inverse Methods for Atmospheric Sounding: Theory and Practice. World Scientific, Singapore, doi: 10.1142/3171.
- Shen, L., R. Gautam, M. Omara, et al., 2022: Satellite quantification of oil and natural gas methane emissions in the US and Canada including contributions from individual basins. *Atmos. Chem. Phys.*, 22, 11203–11215, https://doi.org/10.5194/acp-22-11203-2022.
- Shen, L., D. J. Jacob, R. Gautam, et al., 2023: National quantifications of methane emissions from fuel exploitation using high

- resolution inversions of satellite observations. *Nat. Commun.*, **14**, 4948, https://doi.org/10.1038/s41467-023-40671-6.
- Shephard, M. W., and K. E. Cady-Pereira, 2015: Cross-track Infrared Sounder (CrIS) satellite observations of tropospheric ammonia. *Atmos. Meas. Tech.*, 8, 1323–1336, https://doi.org/10.5194/amt-8-1323-2015.
- Shu, L., L. Zhu, J. Bak, et al., 2022: Improved ozone simulation in East Asia via assimilating observations from the first geostationary air-quality monitoring satellite: Insights from an observing system simulation experiment. *Atmos. Environ.*, **274**, 119003, https://doi.org/10.1016/j.atmosenv.2022.119003.
- Sitwell, M., M. W. Shephard, Y. Rochon, et al., 2022: An ensemble-variational inversion system for the estimation of ammonia emissions using CrIS satellite ammonia retrievals. *Atmos. Chem. Phys.*, 22, 6595–6624, https://doi.org/10.5194/acp-22-6595-2022.
- Su, W. J., C. Liu, Q. H. Hu, et al., 2022: First global observation of tropospheric formaldehyde from Chinese GaoFen-5 satellite: Locating source of volatile organic compounds. *Environ. Pollut.*, 297, 118691, https://doi.org/10.1016/j.envpol.2021.118691
- Sun, W. F., L. Zhu, I. De Smedt, et al., 2021: Global significant changes in formaldehyde (HCHO) columns observed from space at the early stage of the COVID-19 pandemic. *Geophys. Res. Lett.*, **48**, 2e020GL091265, https://doi.org/10.1029/2020GL091265.
- Suto, H., F. Kataoka, N. Kikuchi, et al., 2021: Thermal and near-infrared sensor for carbon observation Fourier transform spectrometer-2 (TANSO-FTS-2) on the Greenhouse gases Observing SATellite-2 (GOSAT-2) during its first year in orbit. *Atmos. Meas. Tech.*, **14**, 2013–2039, https://doi.org/10.5194/amt-14-2013-2021.
- Tang, T., T. H. Cheng, H. Zhu, et al., 2024a: Quantifying instantaneous nitrogen oxides emissions from power plants based on space observations. *Sci. Total Environ.*, 938, 173479, https:// doi.org/10.1016/j.scitotenv.2024.173479.
- Tang, T., L. L. Zhang, H. Zhu, et al., 2024b: Quantifying urban daily nitrogen oxide emissions from satellite observations. *At*mosphere, 15, 508, https://doi.org/10.3390/atmos15040508.
- Tang, Z. J., Z. Jiang, J. Q. Chen, et al., 2023: The capabilities of the adjoint of GEOS-Chem model to support HEMCO emission inventories and MERRA-2 meteorological data. *Geosci. Model Dev.*, 16, 6377–6392, https://doi.org/10.5194/gmd-16-6377-2023.
- Thackeray, C. W., A. Hall, J. Norris, et al., 2022: Constraining the increased frequency of global precipitation extremes under warming. *Nat. Climate Change*, **12**, 441–448, https://doi.org/10.1038/s41558-022-01329-1.
- Theys, N., I. De Smedt, J. Van Gent, et al., 2015: Sulfur dioxide vertical column DOAS retrievals from the Ozone Monitoring Instrument: Global observations and comparison to groundbased and satellite data. *J. Geophys. Res. Atmos.*, 120, 2470–2491, https://doi.org/10.1002/2014JD022657.
- Theys, N., I. De Smedt, H. Yu, et al., 2017: Sulfur dioxide retrievals from TROPOMI onboard Sentinel-5 Precursor: Algorithm theoretical basis. *Atmos. Meas. Tech.*, **10**, 119–153, https://doi.org/10.5194/amt-10-119-2017.
- Tian, Y., Y. W. Sun, T. Borsdorff, et al., 2022a: Quantifying CO emission rates of industrial point sources from Tropospheric

- Monitoring Instrument observations. *Environ. Res. Lett.*, **17**, 014057, https://doi.org/10.1088/1748-9326/ac3b1a.
- Tian, Y., C. Liu, Y. W. Sun, et al., 2022b: Satellite observations reveal a large CO emission discrepancy from industrial point sources over China. *Geophys. Res. Lett.*, 49, e2021GL0973 12, https://doi.org/10.1029/2021GL097312.
- Tu, Q. S., F. Hase, K. Qin, et al., 2024: Quantifying CH₄ emissions from coal mine aggregation areas in Shanxi, China, using TROPOMI observations and the wind-assigned anomaly method. *Atmos. Chem. Phys.*, 24, 4875–4894, https://doi.org/10.5194/acp-24-4875-2024.
- van Geffen, J., K. F. Boersma, H. Eskes, et al., 2020: S5P TRO-POMI NO₂ slant column retrieval: Method, stability, uncertainties and comparisons with OMI. *Atmos. Meas. Tech.*, **13**, 1315–1335, https://doi.org/10.5194/amt-13-1315-2020.
- Wang, F., J. Wang, J. Zhai, et al., 2021: Emission improvements of reactive VOCs based on satellite observations and their impact on ozone simulations. *China Environ. Sci.*, 41, 2504–2514, https://doi.org/10.19674/j.cnki.issn1000-6923.20 21.0262. (in Chinese)
- Wang, H. M., F. Jiang, J. Wang, et al., 2019: Terrestrial ecosystem carbon flux estimated using GOSAT and OCO-2 XCO₂ retrievals. *Atmos. Chem. Phys.*, **19**, 12,067–12,082, https://doi.org/10.5194/acp-19-12067-2019.
- Wang, H. M., F. Jiang, Y. Liu, et al., 2022: Global terrestrial ecosystem carbon flux inferred from TanSat XCO₂ retrievals. *J. Remote. Sens.*, 2022, 9816536, https://doi.org/10.34133/2022/9816536.
- Wang, J., L. Feng, P. I. Palmer, et al., 2020: Large Chinese land carbon sink estimated from atmospheric carbon dioxide data. *Nature*, 586, 720–723, https://doi.org/10.1038/s41586-020-2849-9.
- Wang, J., F. Jiang, W. M. Ju, et al., 2022: Enhanced India-Africa carbon uptake and Asia-Pacific carbon release associated with the 2019 extreme positive Indian Ocean dipole. *Geophys. Res. Lett.*, 49, e2022GL100950, https://doi.org/10.1029/2022GL10 0950.
- Wang, Q., Y. M. Wang, N. Xu, et al., 2024: Preflight spectral calibration of the ozone monitoring suite-nadir on FengYun 3F satellite. *Remote Sens.*, 16, 1538, https://doi.org/10.3390/rs16091538.
- Wang, S. J., J. T. Lin, H. Kong, et al., 2024: Comparison of satellite-based fast inversion methods for nitrogen oxides emissions. *Adv. Earth Sci.*, **39**, 269–278, https://doi.org/10.11867/j.issn.1001-8166.2024.014. (in Chinese)
- Wang, S. W., Q. Zhang, R. V. Martin, et al., 2015: Satellite measurements oversee China's sulfur dioxide emission reductions from coal-fired power plants. *Environ. Res. Lett.*, 10, 1140 15, https://doi.org/10.1088/1748-9326/10/11/114015.
- Wang, W. N., R. Van Der A, J. Y. Ding, et al., 2021: Spatial and temporal changes of the ozone sensitivity in China based on satellite and ground-based observations. *Atmos. Chem. Phys.*, 21, 7253–7269, https://doi.org/10.5194/acp-21-7253-2021.
- Wang, Y., J. Wang, X. G. Xu, et al., 2016: A new approach for monthly updates of anthropogenic sulfur dioxide emissions from space: Application to China and implications for air quality forecasts. *Geophys. Res. Lett.*, 43, 9931–9938, https:// doi.org/10.1002/2016GL070204.
- Wang, Y., J. Wang, M. Zhou, et al., 2020: Inverse modeling of

- SO_2 and NO_x emissions over China using multisensor satellite data Part 2: Downscaling techniques for air quality analysis and forecasts. *Atmos. Chem. Phys.*, **20**, 6651–6670, https://doi.org/10.5194/acp-20-6651-2020.
- Wang, Y. L., P. Ciais, G. Broquet, et al., 2019: A global map of emission clumps for future monitoring of fossil fuel CO₂ emissions from space. *Earth Syst. Sci. Data*, 11, 687–703, https://doi.org/10.5194/essd-11-687-2019.
- Wang, Y. L., G. Broquet, F. M. Bréon, et al., 2020: PMIF v1.0: Assessing the potential of satellite observations to constrain CO₂ emissions from large cities and point sources over the globe using synthetic data. *Geosci. Model Dev.*, **13**, 5813–5831, https://doi.org/10.5194/gmd-13-5813-2020.
- Warner, J. X., Z. G. Wei, L. L. Strow, et al., 2016: The global tropospheric ammonia distribution as seen in the 13-year AIRS measurement record. *Atmos. Chem. Phys.*, 16, 5467–5479, https://doi.org/10.5194/acp-16-5467-2016.
- Watine-Guiu, M., D. J. Varon, I. Irakulis-Loitxate, et al., 2023: Geostationary satellite observations of extreme and transient methane emissions from oil and gas infrastructure. *Proc. Natl. Acad. Sci. USA*, **120**, e2310797120, https://doi.org/10.1073/pnas.2310797120.
- Wei, Y. X., X. Y. Zhang, and H. Zhang, 2023: Spatial and temporal distribution of sulfur dioxide and main emission sources in China. *China Environ. Sci.*, **43**, 5678–5686, https://doi.org/10.3969/j.issn.1000-6923.2023.11.006. (in Chinese)
- Weismann, D., M. Möckel, H. Paeth, et al., 2023: Modelling variations of emergency attendances using data on community mobility, climate and air pollution. *Sci. Rep.*, 13, 20595, https://doi.org/10.1038/s41598-023-47857-4.
- Wen, P., C. Zhang, Q. Yang, et al., 2024: Characterization of spatial and temporal distribution of NH₃ concentrations and emissions in China based on IASI observations. *China Environ. Sci.*, **44**, 3040–3051, https://doi.org/10.19674/j.cnki.issn1000-6923,20240206.008. (in Chinese)
- Wu, C.-Y., X.-Y. Zhang, L.-F. Guo, et al., 2023: An inversion model based on GEOS-Chem for estimating global and China's terrestrial carbon fluxes in 2019. *Adv. Clim. Chang. Res.*, 14, 49–61, https://doi.org/10.1016/j.accre.2023.01.001.
- Wu, D. E., J. C. Lin, T. Oda, et al., 2020: Space-based quantification of per capita CO₂ emissions from cities. *Environ. Res. Lett.*, **15**, 035004, https://doi.org/10.1088/1748-9326/ab68eb.
- Xia, C. Z., C. Liu, Z. N. Cai, et al., 2021: First sulfur dioxide observations from the environmental trace gases monitoring instrument (EMI) onboard the GeoFen-5 satellite. *Sci. Bull.*, **66**, 969–973, https://doi.org/10.1016/j.scib.2021.01.018.
- Xie, Y., W. Wang, Y. Chen, et al., 2024: NH₃ emissions and lifetime estimated by satellite observations with differential evolution algorithm. *Atmosphere*, **15**, 251, https://doi.org/10.3390/ atmos15030251.
- Xing, J., S. W. Li, S. X. Zheng, et al., 2022: Rapid inference of nitrogen oxide emissions based on a top-down method with a physically informed variational autoencoder. *Environ. Sci. Technol.*, **56**, 9903–9914, https://doi.org/10.1021/acs.est.1c08 337.
- Xu, F. J., Q. X. Huang, H. B. Yue, et al., 2023: The challenge of population aging for mitigating deaths from PM_{2.5} air pollution in China. *Nat. Commun.*, **14**, 5222, https://doi.org/10.1038/s41467-023-40908-4.

- Xu, T. Y., C. X. Zhang, J. K. Xue, et al., 2024: Estimating hourly nitrogen oxide emissions over East Asia from geostationary satellite measurements. *Environ. Sci. Technol. Lett.*, 11, 122– 129, https://doi.org/10.1021/acs.estlett.3c00467.
- Xue, R. B., S. S. Wang, S. B. Zhang, et al., 2022: Estimating city NO_x emissions from TROPOMI high spatial resolution observations—a case study on Yangtze River Delta, China. *Urban Climate*, 43, 101150, https://doi.org/10.1016/j.uclim.2022. 101150.
- Yang, D. X., H. F. Zhang, Y. Liu, et al., 2017: Monitoring carbon dioxide from space: Retrieval algorithm and flux inversion based on GOSAT data and using CarbonTracker-China. Adv. Atmos. Sci., 34, 965–976, https://doi.org/10.1007/s00376-017-6221-4.
- Yang, D. X., Y. Liu, L. Feng, et al., 2021: The first global carbon dioxide flux map derived from TanSat measurements. *Adv. Atmos. Sci.*, 38, 1433–1443, https://doi.org/10.1007/s00376-021-1179-7.
- Yang, K., R. R. Dickerson, S. A. Carn, et al., 2013: First observations of SO₂ from the satellite Suomi NPP OMPS: Widespread air pollution events over China. *Geophys. Res. Lett.*, 40, 4957–4962, https://doi.org/10.1002/grl.50952.
- Yang, Y., Y. Zhao, L. Zhang, 2019a: Evaluating the influence of satellite observation on inversing NO_x emission at regional scale. *Int. Arch. Photogramm., Remote Sens. Spatial Inf. Sci.*, XLII-3/W9, 211–217, https://doi.org/10.5194/isprs-archives-XLII-3-W9-211-2019.
- Yang, Y., Y. Zhao, L. Zhang, et al., 2019b: Evaluating the methods and influencing factors of satellite-derived estimates of NO_x emissions at regional scale: A case study for Yangtze River Delta, China. *Atmos. Environ.*, **219**, 117051, https://doi.org/10.1016/j.atmosenv.2019.117051.
- Yang, Y., Y. Zhao, L. Zhang, et al., 2021: Improvement of the satellite-derived NO_x emissions on air quality modeling and its effect on ozone and secondary inorganic aerosol formation in the Yangtze River Delta, China. *Atmos. Chem. Phys.*, 21, 1191–1209, https://doi.org/10.5194/acp-21-1191-2021.
- Yao, L., D. X. Yang, Z. N. Cai, et al., 2022: Status and trend analysis of atmospheric methane satellite measurement for carbon neutrality and carbon peaking in China. *Chinese J. Atmos. Sci.*, 46, 1469–1483, https://doi.org/10.3878/j.issn.1006-9895.2207.22096. (in Chinese)
- Zeng, Z. C., L. Lee, C. L. Qi, et al., 2023: Optimal estimation retrieval of tropospheric ammonia from the Geostationary Interferometric Infrared Sounder on board FengYun-4B. *Atmos. Meas. Tech.*, **16**, 3693–3713, https://doi.org/10.5194/amt-16-3693-2023.
- Zhang, C. X., C. Liu, K. L. Chan, et al., 2020: First observation of tropospheric nitrogen dioxide from the Environmental Trace Gases Monitoring Instrument onboard the GaoFen-5 satellite. *Light: Sci. Appl.*, 9, 66, https://doi.org/10.1038/s41377-020-0306-z.
- Zhang, J., A. Li, P. H. Xie, et al., 2015: Research on the spatial/temporal patterns of NO₂ concentration and NO_x emissions of Lanzhou by applying satellite data. *China Environ. Sci.*, **35**, 2291–2297, https://doi.org/10.3969/j.issn.1000-6923.2015.08. 006. (in Chinese)
- Zhang, L., Y. F. Chen, Y. H. Zhao, et al., 2018: Agricultural ammonia emissions in China: Reconciling bottom-up and top-

- down estimates. *Atmos. Chem. Phys.*, **18**, 339–355, https://doi.org/10.5194/acp-18-339-2018.
- Zhang, L. Y., F. Jiang, W. He, et al., 2023: A robust estimate of continental-scale terrestrial carbon sinks using GOSAT XCO₂ retrievals. *Geophys. Res. Lett.*, 50, e2023GL102815, https:// doi.org/10.1029/2023GL102815.
- Zhang, P., X. Q. Hu, Q. F. Lu, et al., 2021: FY-3E: The first operational meteorological satellite mission in an early morning orbit. Adv. Atmos. Sci., 39, 1–8., https://doi.org/10.1007/s00376-021-1304-7.
- Zhang, Q. Q., K. F. Boersma, B. Zhao, et al., 2023: Quantifying daily NO_x and CO₂ emissions from Wuhan using satellite observations from TROPOMI and OCO-2. *Atmos. Chem. Phys.*, **23**, 551–563, https://doi.org/10.5194/acp-23-551-2023.
- Zhang, R. X., Y. Z. Zhang, and H. P. Lin, et al., 2020: NO_x emission reduction and recovery during COVID-19 in East China. *Atmosphere*, **11**, 433, https://doi.org/10.3390/atmos11040433.
- Zhang, S. Q., L. P. Lei, H. Song, et al., 2023: A neural network partitioning method for carbon emission estimation based on spatial–temporal clustering of atmospheric CO₂ concentration. *China Environ. Sci.*, **43**, 5604–5613, https://doi.org/10.19674/j.cnki.issn1000-6923.20230628.006. (in Chinese)
- Zhang, X. Y., P. Zhang, Y. Zhang, et al., 2007: The trend, seasonal cycle, and sources of tropospheric NO₂ over China during 1997–2006 based on satellite measurement. *Science in China Series D: Earth Sciences*, **50**, 1877–1884, https://doi.org/10.1007/s11430-007-0141-6.
- Zhang, Y. Z., R. Gautam, S. Pandey, et al., 2020: Quantifying methane emissions from the largest oil-producing basin in the United States from space. *Sci. Adv.*, **6**, eaaz5120, https://doi.org/10.1126/sciadv.aaz5120.
- Zhang, Y. Z., D. J. Jacob, X. Lu, et al., 2021: Attribution of the accelerating increase in atmospheric methane during 2010–2018 by inverse analysis of GOSAT observations. *Atmos. Chem. Phys.*, **21**, 3643–3666, https://doi.org/10.5194/acp-21-3643-2021.
- Zhang, Y. Z., S. X. Fang, J. M. Chen, et al., 2022: Observed changes in China's methane emissions linked to policy drivers. *Proc. Natl. Acad. Sci. USA*, **119**, e2202742119, https://doi.org/10.1073/pnas.2202742119.
- Zhang, Y. Z., H. Q. Mao, C. H. Chen, et al., 2024: Application of satellite observations to verify methane emission inventories. *Natl. Remote Sens. Bull.*, **28**, 1940–1954, https://doi.org/10.11834/jrs.20243350. (in Chinese)
- Zhao, M., X. J. Tian, Y. L. Wang, et al., 2024: Slow down in China's methane emission growth. *Natl. Sci. Rev.*, 11, nwae223, https://doi.org/10.1093/nsr/nwae223.
- Zheng, B., F. Chevallier, P. Ciais, et al., 2018: Rapid decline in carbon monoxide emissions and export from East Asia between years 2005 and 2016. *Environ. Res. Lett.*, 13, 044007, https://doi.org/10.1088/1748-9326/aab2b3.
- Zheng, B., F. Chevallier, P. Ciais, et al., 2020a: Observing carbon

- dioxide emissions over China's cities and industrial areas with the Orbiting Carbon Observatory-2. *Atmos. Chem. Phys.*, **20**, 8501–8510, https://doi.org/10.5194/acp-20-8501-2020.
- Zheng, B., G. N. Geng, P. Ciais, et al., 2020b: Satellite-based estimates of decline and rebound in China's CO₂ emissions during COVID-19 pandemic. *Sci. Adv.*, 6, eabd4998, https://doi.org/10.1126/sciadv.abd4998.
- Zheng, B., P. Ciais, F. Chevallier, et al., 2021: Increasing forest fire emissions despite the decline in global burned area. *Sci. Adv.*, 7, eabh2646, https://doi.org/10.1126/sciadv.abh2646.
- Zheng, B., P. Ciais, F. Chevallier, et al., 2023: Record-high CO₂ emissions from boreal fires in 2021. *Science*, **379**, 912–917, https://doi.org/10.1126/science.ade0805.
- Zhong, J. T., X. Y. Zhang, L. F. Guo, et al., 2023: Ongoing CO₂ monitoring verify CO₂ emissions and sinks in China during 2018–2021. *Sci. Bull.*, **68**, 2467–2476., https://doi.org/10.1016/j.scib.2023.08.039.
- Zhou, B. N., H. Guo, Y. Zeren, et al., 2023: An observational constraint of VOC emissions for air quality modeling study in the Pearl River Delta region. *J. Geophys. Res. Atmos.*, 128, e2022JD038122, https://doi.org/10.1029/2022JD038122.
- Zhu, L., D. K. Henze, K. E. Cady-Pereira, et al., 2013: Constraining U.S. ammonia emissions using TES remote sensing observations and the GEOS-Chem adjoint model. *J. Geophys. Res. Atmos.*, 118, 3355–3368, https://doi.org/10.1002/jgrd.50166.
- Zhu, L., D. J. Jacob, L. J. Mickley, et al., 2014: Anthropogenic emissions of highly reactive volatile organic compounds in eastern Texas inferred from oversampling of satellite (OMI) measurements of HCHO columns. *Environ. Res. Lett.*, 9, 114004, https://doi.org/10.1088/1748-9326/9/11/114004.
- Zhu, S. H., L. Feng, Y. Liu, et al., 2022: Decadal methane emission trend inferred from proxy GOSAT XCH₄ retrievals: Impacts of transport model spatial resolution. *Adv. Atmos. Sci.*, 39, 1343–1359, https://doi.org/10.1007/s00376-022-1434-6.
- Zhu, Y. Z., Q. H. Hu, M. Gao, et al., 2021: Quantifying contributions of local emissions and regional transport to NO_x in Beijing using TROPOMI constrained WRF-chem simulation. *Remote Sens.*, **13**, 1798, https://doi.org/10.3390/rs13091798.
- Zhu, Y. Z., C. Liu, Q. H. Hu, et al., 2022: Impacts of TROPOMIderived NO_x emissions on NO₂ and O₃ simulations in the NCP during COVID-19. *ACS Environ. Au*, **2**, 441–454, https://doi. org/10.1021/acsenvironau.2c00013.
- Zoogman, P., X. Liu, R. M. Suleiman, et al., 2017: Tropospheric emissions: Monitoring of pollution (TEMPO). *J. Quant. Spectrosc. Radiat. Transfer*, **186**, 17–39, https://doi.org/10.1016/j.jqsrt.2016.05.008.
- Zuo, X. X., W. F. Sun, I. De Smedt, et al., 2023: Observing downwind structures of urban HCHO plumes from space: Implications to non-methane volatile organic compound emissions. *Geophys. Res. Lett.*, **50**, e2023GL106062, https://doi.org/10.1029/2023GL106062.